Dalton Transactions

ROYAL SOCIETY OF CHEMISTRY

FRONTIER

View Article Online
View Journal | View Issue

Cite this: *Dalton Trans.*, 2025, **54**, 38

Recent advances in the syntheses and emerging applications of 2D borophene-based nanomaterials with a focus on supercapacitors

Prashanta Pal * and Mahasweta Nandi *

Two-dimensional (2D) nanosheets of boron, *i.e.* borophene, have triggered interest in progressive research as a result of the vast field of opportunities to explore, from its innovative synthetic techniques to novel properties and potential applications. It possesses exceptional tuneable properties such as mechanical flexibility, electronic and thermal conductivity, optical transparency, metallicity, anisotropy and polymorphism. This has sparked significant curiosity in the application of borophene-based materials in energy storage systems such as supercapacitors, which display high-power density with reliable energy density, fast charge/discharge kinetics and long cycle life. This review comprehensively discusses the recent progress in the different techniques for borophene synthesis (chemical vapor deposition, molecular beam epitaxy, segregation-enhanced epitaxy, van der Waals epitaxy, ultrasound-assisted liquid phase exfoliation, mechanical exfoliation, electrochemical exfoliation and modified Hummers' method) including the resultant phases, its properties (mechanical, thermal, electronic and magnetic) and potential applications of borophene/borophene composites in supercapacitors with their charge storage mechanisms. This article mainly focuses on the literature published since 2015 when the first laboratory synthesis of borophene was accomplished. Featuring over 50 articles, the present contribution offers insightful information, suggestions and discussions on the issues and challenges involved in future research in this direction.

Received 9th September 2024,
Accepted 11th November 2024

DOI: 10.1039/d4dt02573c

rsc.li/dalton

Introduction

The blooming of energy storage technology has fundamentally made our daily lives easier.[1] With the rapidly growing environ-

Integrated Science Education and Research Centre, Siksha Bhavana, Visva-Bharati University, Santiniketan 731 235, India. E-mail: prashantapal7991@gmail.com, mahasweta.nandi@visva-bharati.ac.in

Prashanta Pal

Prashanta Pal completed his B.Sc. (Honours in Chemistry) in 2018 and M.Sc. (Inorganic Chemistry Specialization) in 2020 from The University of Burdwan, West Bengal, India. Currently, he is pursuing Ph.D. under the supervision of Dr Mahasweta Nandi at Integrated Science Education and Research Centre, Visva-Bharati, Santiniketan. His research interest focuses on the syntheses of advanced porous functional materials and their applications in the field of energy storage.

Mahasweta Nandi

Mahasweta Nandi is currently an assistant professor at the Integrated Science Education and Research Centre, Visva-Bharati, Santiniketan. She received her Ph.D. degree working at the Indian Association for the Cultivation of Science, Kolkata in 2008. She received GCOE and JSPS post-doctoral fellowships at the Osaka University, Japan during 2010–2012. She has co-authored more than 90 research articles so far. Her research interests include application of different types of porous materials in metal-ion sensing and separation, energy storage devices, adsorption and catalysis.

mental pollution and depletion of non-renewable energy sources, it is essential to store clean energy, *i.e.* renewable energy. Due to the intermittent and fluctuating power output of these energy sources, energy storage systems such as rechargeable batteries and electrochemical capacitors are in high demand.[2,3] Supercapacitors as electrochemical energy-storage devices have received considerable attention due to their potential advantages, such as long cycle lifetime, quick charge/discharge, excellent power density with considerable energy density, lightweight nature, flexibility as well as environmental friendliness.[4,5] In this quest, two-dimensional (2D) nanomaterials have gained widespread interest due to their distinctive structural properties, high surface-to-volume ratios and tuneable electronic and electrochemical properties.[6,7] These materials have attracted attention across a host of research domains, impacting critical sectors such as catalysis,[8] energy storage,[9] solar cells,[10] flexible electronics and sensors.[11] In the year 2004, the discovery of graphene, a revolutionary 2D material[12] by virtue of its remarkable performance and potential applications, generated a tremendous research interest in the field of 2D materials. Owing to their special and novel physical and chemical properties, 2D materials such as graphene,[13] phosphorene,[14] transition metal dichalcogenides (TMDs),[15] 2D metal carbides and nitrides (MXenes),[16] hexagonal boron nitride (h-BN)[17] and black phosphorus[18] have been found to be promising players in various areas of basic science as well as advanced technology. Borophene (BP), first experimentally synthesized by Mannix *et al.*,[19] is a new monoelemental 2D nanosheet of boron (B), which triggered interest due to its exceptional chemical, electronic, superconductive and thermal properties; anisotropy; mechanical flexibility; optical transparency; transport properties; metallicity and presence of massless Dirac fermions (Fig. 1).[20,21] The existence of BP in different structural phases bestow them with the option of a wide range of bandgap,[20] which offers great prospect in bridging the gap between semi-metallic zero-bandgap graphene, large-bandgap transition metal dichalcogenides and insulating boron nitrides. In comparison to few-layered black phosphorus, some typical BPs have displayed good stability under ambient conditions or even in acidic or basic solvents.[22,23] Also, dispersions of hydrogenated borophene (borophane) in strong acid and base show remarkable stability, which ensures its integrity under harsh conditions. This is crucial for its potential applications in various advanced nanoelectronic devices.[24]

Boron (B) and carbon (C) have somewhat similar chemistry due to their adjacent occupancy in the periodic table. However, due to the electron-deficient character of B, its bonding mechanism is more complex than C and it forms '3c–2e' bonds, resulting in structural polymorphism with diverse properties. Depending on the size, B clusters are present in quasiplanar, planar or cage-like configurations. Typically, clusters of small size ($n < 15$) exist as planar or quasiplanar structures analogous to those of carbon-like aromatic/anti-aromatic molecules. However, the larger B clusters ($n \geq 28$) exist in cage-like conformations having similar structure and symmetry *vis-à-vis* their carbon analogues.[25] The most widely studied allotropic forms of BP are 2-*Pmmn*, β_{12}, χ_3 and honeycomb,[26] whose atomic structures are given in Fig. 2. The β_{12} and χ_3 phases maintain planarity while the 2-*Pmmn* phase of BP has an

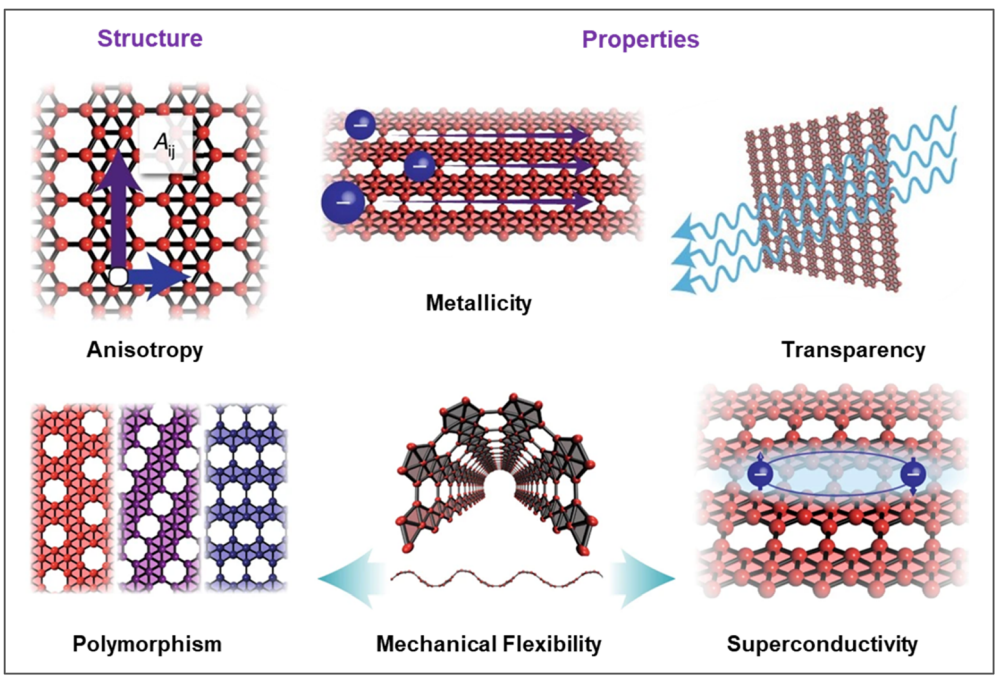

Fig. 1 Summary of structure and properties of borophene (A_{ij} denotes a generic anisotropic property tensor component). Reproduced with permission. Copyright 2018, Springer Nature.[20]

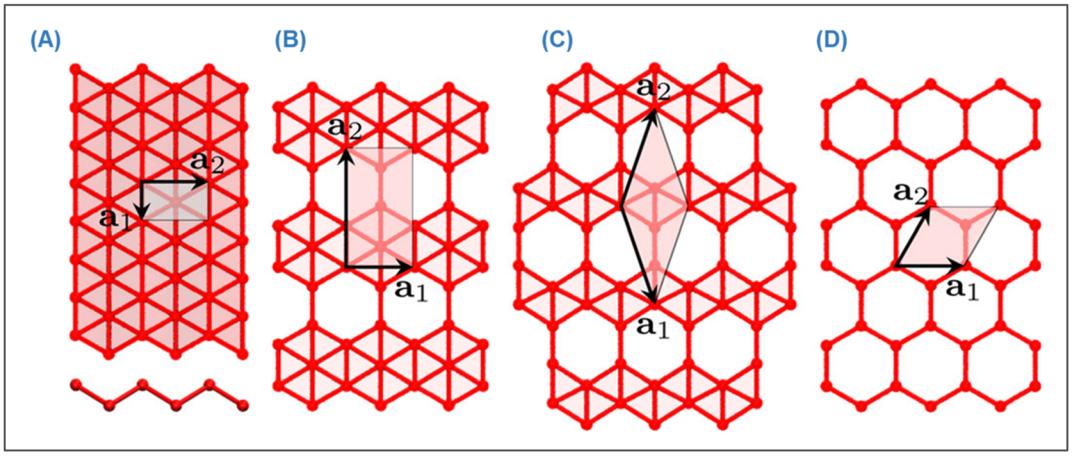

Fig. 2 Atomic structure of the allotropic forms of borophene. (A) 2-*Pmmn*, (B) β_{12}, (C) χ_3 and (D) honeycomb with the unit cell and lattice vector a_1 and a_2. Reproduced with permission. Copyright 2016, American Chemical Society.[26]

undulating structure with a buckling height of 0.91 Å. The honeycomb structure of BP resembles that of graphene.[27] All these four phases of BP are metallic in nature, which originate from their delocalized multicentre bonding electrons. Among these, χ_3 is the phase that exists at higher temperatures whereas β_{12} is the metastable phase. Compared to graphene, the β_{12} phase of BP possesses high carrier density and a higher Young's modulus.[28] BP shows a vast diversity of atomic structures depending on its hexagonal hole density (d_H), which is the number of hexagonal holes per boron atom in the pristine triangular sheet. The stability of the BP polymorphs depends on the d_H. While the structures with $d_H > 1/9$ are planar, electron-deficient and tend to withdraw the electron density from the surrounding atoms, thereby stabilizing their structure, boron sheets with $d_H < 1/9$ are electron-rich and assume buckled structures resulting from the off-plane and in-plane mixing of the orbitals. The d_H values of the different polymorphs of BP, *i.e.*, 2-*Pmmn*, β_{12}, χ_3 and honeycomb structures, are 0, 1/6, 1/5 and 1/3, respectively.[27] For a d_H value of *ca.* 1/9, the highly stable α′ phase is favoured, while d_H values of *ca.* 1/7 – 5/33 lead to the β_{31}, β_{32} and β_{33} phases having similar brick-wall motifs but differing in their periodicities.[29]

The synthesis of a monolayer of boron is not straightforward because in the bulk form, there remains a strong metallic force that confers it high stability. Unlike graphene, in the bulk form of boron, no layered structure exists; as a result, the synthesis of 2D-borophene becomes quite challenging. Nevertheless, the untiring efforts of scientists have led to the invention of different synthetic methods, thereby making the synthesis of 2D-borophenes a reality now. There are several synthetic strategies such as chemical vapor deposition (CVD), molecular beam epitaxy (MBE), segregation-enhanced epitaxy (SEE), van der Waals epitaxy (vdWE), different exfoliation techniques, and modified Hummers' method to achieve the synthesis of borophenes. Due to the unique physicochemical properties and tuneable electronic and electrochemical features of this 2D nanomaterial, it has become a promising player in the field of energy storage and conversion. The metallicity, outstanding electrical conductivity, chemical stability, good mechanical strength, low diffusion barrier and lightweight of the borophenes make them suitable for applications in energy storage devices.[23,25,29,30] Additionally, the bandgap of BP may be modulated by applying shear strain and can reach up to 0.538 eV.[31] This tunability of the band gap is crucial for modulating the electronic properties and hence the potential use of these materials in devices requiring a specific bandgap. The theoretical capacitance value of the nanosheets of 2D boron is 400 F g^{-1}, four times that of graphene, which makes them potential candidates for supercapacitor electrodes.[32] Current research interests are focussed on the unique properties of 2D heterostructures, involving direct interactions of chemically distinct components. The interfaces of these components play a very crucial role in boosting the charge storage abilities of the heterostructures by means of synergistic effects. Nevertheless, the fabrication of stable heterostructures in itself has its own set of challenges. BP has the potential to form heterostructures with other functional materials because of its polymorphism and diverse bonding geometries. Structures such as graphene,[33] MXene,[34] poly(3,4-ethylenedioxythiophene):polystyrene sulfonate (PEDOT:PSS)[35] and polyaniline (PANI)[36] offer chances to modify the characteristics of BP and enhance its performance in energy storage systems.

There are review articles that discuss the evolution of borophene[37] and the syntheses,[20] structure, properties and overall applications of borophenes and borophene-based nanosheets.[21,25] Some articles have concentrated on their applications in the field of environment and energy,[23,27,29] information technology and sensing/biosensing,[23,38] biomedicine[39] and hydrogen storage.[40] This review article distinguishes itself by focusing on the recent advancements and latest developments in the synthesis strategies of borophenes and exploring the current advancements in their unique properties. It particularly highlights BP as a promising material for energy storage in next-generation supercapacitors with

high energy storage ability, mechanical flexibility and extraordinary recyclability, addressing current challenges and offering insightful information for future advancements in this field.

Different synthesis strategies of borophene

The fabrication of high-quality 2D borophene sheets from the bulk boron phase is quite a challenging task. For the successful implementation of BP in advanced applications, it is important to find out and establish effective approaches for its sustainable, cost-effective and large-scale production. High crystallinity should be ensured to attain the desired mechanical, chemical and electronic properties that make BP befitting for various applications in electronics, catalysis, energy storage, *etc*. BP has been developed *via* bottom-up (chemical vapor deposition, physical vapour deposition, electrochemical deposition, *etc*.) as well as top-down (liquid phase exfoliation, mechanical exfoliation and other exfoliation techniques) synthetic processes. A summary of the various synthetic routes is given in Table 1.

Bottom-up synthesis of borophene

Chemical vapor deposition (CVD)

In the CVD method, achieving high-quality, superior, large area, uniform BP sheet involves the cautious supervision of different parameters such as temperature, pressure, substrate selection, precursors, and gas flow. In this method, the thermally decomposed boron atoms from the precursor are deposited on the surface of the substrate. CVD is one of the most promising approaches for the extensive manufacturing of BP (Fig. 3), though it needs sophisticated machinery and accurate optimization of the growth conditions of the boron film.

Tai and co-workers[41] prepared BP nanosheet on the surface of carbon cloth *via* the CVD method (Fig. 3A–D). The synthesis was achieved by taking bulk sodium borohydride ($NaBH_4$) as the boron source and hydrogen as the carrier gas. The crystal structure of the BP nanosheet obtained closely resembled a theoretical α′-borophene nanosheet. The optimized growth

Table 1 Summary of the various synthetic routes and application of borophenes (BP)

Synthesis technique	Boron source	Substrate/solvent	Type/phase of produced BP	Application	Ref.
CVD (chemical vapor deposition)	Bulk $NaBH_4$	Carbon cloth surface	α′ phase	Electrocatalytic hydrogen evolution reaction (HER)	41
	B_2H_6 gas	Al-coated Si wafer	χ_3 with some β_{12}	Supercapacitor	42
	Boron powder/ B_2O_3	Cu foil	Tetragonal BP sheets	Electrical transport and field emission	43
	B_2H_6 gas	Al-coated Si wafer	χ_3 with some β_{12}	—	44
MBE (molecular beam epitaxy)	Boron rod	Ag(111)	Atomically thin BP sheet	—	19
	Pure boron	Ag(111)	β_{12} and χ_3	—	45
	Pure boron	Cu(111)	β_{12}	—	46
SEE (segregation-enhanced epitaxy)	Borazine	Ir(111)	χ_6	—	47
(**vdWE**) (van der Waals epitaxy)	$NaBH_4$ powder	$KMg_3AlSi_3O_{10}F_2$ mica	α′ 2H-BP sheet	Photodetector	48
LPE (liquid phase exfoliation)	Boron powder	DMF and IPA	Few-layer boron sheets	Supercapacitor	49
	Boron powder	NMP and ethanol	Ultrathin boron nanosheets	Multimodal imaging-guided cancer therapy	50
	Boron powder	IPA	Few layered boron sheets	Photodetector	51
	Boron flakes	Ethanol	β_{12}	Lithium-ion battery	52
	Boron powder	Acetone and IPA	β_{12}, χ_3 and γ orthorhombic	HER	53
	Boron powder	NMP	β_{12} S- and Fe-doped BP	Supercapacitor	54
ME (mechanical exfoliation)	Boron crystal	SiO_2	β_{12} and χ_3	Molecular Sensing	55
	Boron powder	—	β-Rhombohedral, γ-orthorhombic and τ-B	—	56
	Boron powder	DI water	Three-layered BP sheet	—	57
ECE (electrochemical exfoliation)	Boron powder	Cu/Ni metal mesh	β-Rhombohedral in Cu mesh β_{12} and χ_3 in Ni mesh	—	58
	Pure boron rod	—	Few atomic layers of BP	—	59
Modified Hummer's method	Boron flakes	DMF/acetone/IPA/water/ ethylene glycol	β_{12}, χ_3 and their intermediate phase	Photo, gas and molecular sensing	60
	Boron powder	Acidic $KMnO_4$ solution	β-Rhombohedral and oxidized β phase	Supercapacitor	61

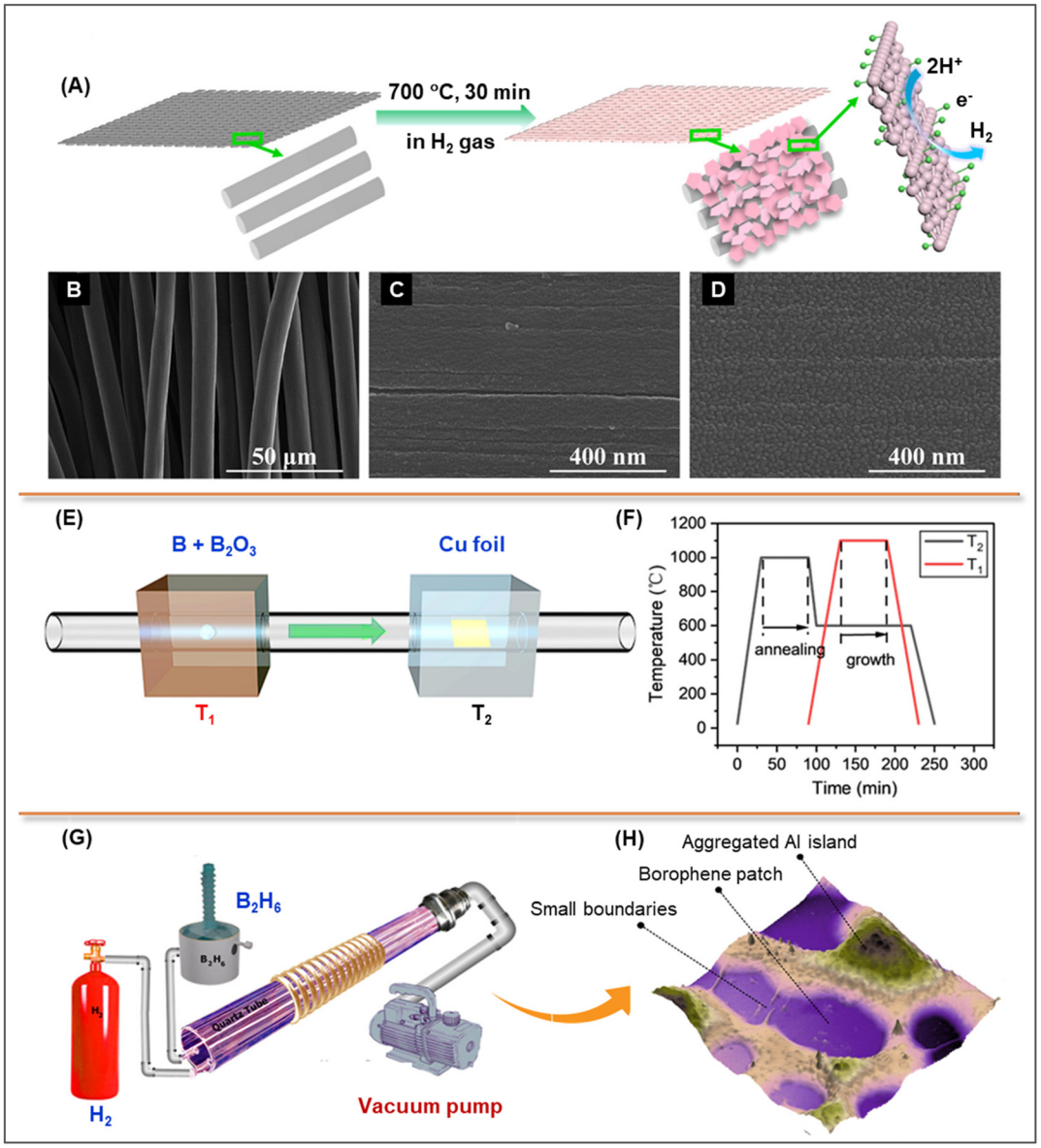

Fig. 3 Schematic diagram of material growth and morphology of the borophene nanosheets by CVD methods. (A) Growth of borophene nanosheets and hydrogen evolution reaction, (B) scanning electron microscopy image of bare carbon cloth and (C and D) high-magnification SEM image of carbon cloth and borophene nanosheets on the surface of carbon cloth. Reproduced with permission. Copyright 2021, American Chemical Society.[41] (E) Two-zone tube furnace system for the growth of borophene sheets and (F) curves of the rising and falling temperatures of the reaction region (T_1) and the substrate region (T_2). Reproduced with permission. Copyright 2023, American Chemical Society.[43] (G) Synthesis setup and (H) AFM topography of borophene nanosheets. Reproduced with permission. Copyright 2024, American Chemical Society.[44]

condition for BP was found to be at 973 K for 30 min, above which the BP sheets were destroyed and below which the grain growth of BP was obstructed due to the lack of sufficient energy for nucleation. The BP thus produced displayed outstanding electrocatalytic hydrogen evolution activity (Tafel slope of 69 mV dec^{-1}), corrosion resistance and cycle stability.

Abdi *et al.*[42] demonstrated an Al-assisted CVD strategy to grow BP on an Al-coated Si wafer substrate under a high vacuum of 3×10^{-3} torr and temperature of 830 K with a continuous flow of H_2 and B_2H_6 gas as the boron source. The measured thickness of the BP sheets was found to be a few angstroms. Atomic force microscopy (AFM) images suggested a statistical distribution of sizes of these BP sheets in all the samples. While the average area was *ca.* 6 μm^2 for the smaller sheets, wider BP sheets with a lateral area of 40–50 μm^2 were also observed. These results indicated the coexistence of primarily the χ_3 phase along with some signs of the β_{12} phase in the resulting BP.

Liu's group[43] developed 2D tetragonal BP sheets, which were highly stable under ambient conditions, *via* the low-pressure CVD (LPCVD) method (Fig. 3E and F). For the growth of BP, a polycrystalline copper foil (25 μm thick) was chosen as the substrate and a mixture of crystalline boron powder and

boron oxide (B_2O_3) in the weight ratio of 5 : 1 were taken as the boron sources. For the generation of boron vapor, the temperature of the reaction vessel was maintained at 1373 K and the flow rate of the reaction gases was kept at 10 SCCM of Ar and 20 SCCM of H_2 (SCCM = standard cubic centimetres per minute). The synthesized BP sheets were planar with dimensions of 1 μm × 1 μm and thickness of ~15 nm. The observed mean electrical conductivity was *ca.* 4.5×10^{-4} S cm^{-1} and the band gap was *ca.* 2.1 eV. These BP sheets retained quite good and stable electrical transport along with field emission performances under ambient pressure.

Rezvani *et al.*[44] used Al layer-deposited (100) silicon wafer substrate for the CVD growth of BP sheets (Fig. 3G and H). The growth temperature was fixed at 830 K with a gas mixture of 25% H_2 and 75% B_2H_6 at flow rates of 40 and 15 SCCM, respectively. The AFM topography on a small region of a single sheet also showed height variations (Fig. 3H), which were attributed to the different number of atomic layers present in a single sheet. It further indicated the presence of small 3D boundaries and aggregated Al particles scattered in the sheets. Raman spectroscopy results revealed the presence of χ_3 as well as a small percentage of the β_{12} phase in the sample after prolonged exposure in an ambient environment. The kernel curve of the overall distribution indicated the existence of one-layer to five-layers of BP sheets, and the thickness of each sheet was estimated to be *ca.* 3.0–3.5 Å.

Physical vapor deposition (PVD)

PVD processes involve the vaporization of the material sources into their gaseous state using some physical methods under high vacuum conditions and their subsequent deposition onto a substrate to obtain a functional film. Different types of epitaxial growth methods constitute this category, which include molecular beam epitaxy, segregation-enhanced epitaxy and van der Waals epitaxy. These epitaxial methods show exceptional potential in the production of high-quality and large-area BP films. The deposition parameters in these techniques can be controlled precisely to obtain various polymorphs of BP including those with multilayer structures and tuneable properties.

Molecular beam epitaxy (MBE)

MBE is a highly regulated process used to deposit very thin layers of materials onto a substrate in an ultra-high vacuum (UHV) environment, forming a crystalline structure. In 2015, Mannix *et al.*,[19] showed for the first time the successful preparation of an atomically thin BP sheet (Fig. 4) under UHV conditions using a clean single crystal Ag(111) substrate with solid boron rod as the atomic source (99.9999% purity). During growth, the samples were heated to 723–973 K and the deposition rate was maintained between 0.01 and 0.1 mL min^{-1}. After deposition, it was confirmed from *in situ* Auger electron spectroscopy (Fig. 4C) that no contamination or alloy formation took place on the Ag(111) substrate. The scanning tunneling microscopy (STM) images of the synthesized BP sheet suggested the presence of two individual boron phases: one is a homogeneous phase and another a more corrugated "striped" phase. Low deposition rates and higher growth temperatures favoured the striped phase while higher deposition rates favoured the homogeneous phase, implying that the homogeneous phase is metastable compared to the striped phase.

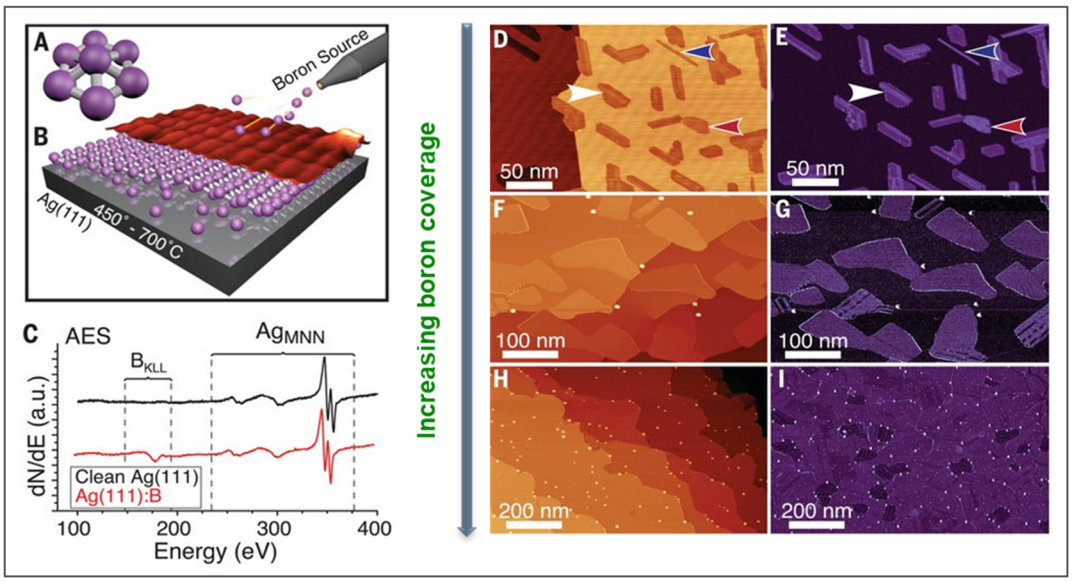

Fig. 4 Growth of borophene sheets by the MBE technique and their atomic-scale characterization. (A) Distorted B_7 cluster, (B) growth setup with atomic structure model and STM topography rendering, (C) Auger electron spectra of clean Ag(111) before and after boron deposition, large-scale STM topography at (D and E) low coverage, (F and G) medium coverage and (H and I) high coverage. Regions of homogeneous-phase, striped-phase island and striped-phase nanoribbon are indicated with red, white and blue arrows, respectively. Reproduced with permission. Copyright 2015, The American Association for the Advancement of Science.[19]

Wu and Chen's group[45] reported the synthesis of BP in a UHV chamber combining an MBE system with a low-temperature STM (4.5 K) operated at a base pressure of 2×10^{-11} torr. The borophenes were grown on a single-crystal Ag(111) substrate and pure boron (99.9999%) was evaporated from an electron-beam evaporator onto the substrate. The pressure during boron growth was greater than 6×10^{-11} torr. It was concluded after experiments and first-principles calculations that two distinct types of 2D boron structures were formed: one was β_{12} sheet and the other was χ_3 sheet. This study also suggested that there existed weak interaction between the boron sheets and the Ag(111) substrate surface because both the β_{12} sheet and the χ_3 sheet retained their isolated planar forms after adsorption on Ag(111). The formation of the boron sheet was highly dependent on the substrate temperature; when the substrate temperature during growth was less than 500 K, only clusters or disordered structures were formed. At the substrate temperature of *ca.* 570 K, the β_{12} sheet structure was observed and at temperatures higher than 800 K, only the χ_3 sheet was found. The same group in 2022[46] successfully synthesized large-sized, single-crystalline bilayer BP sheets on the surface of Cu(111) substrate. Through an electron-beam evaporator, boron atoms were evaporated onto the surface of Cu(111) at various substrate temperatures. Within the temperature window of 600–750 K, bilayer BP was formed, which was narrower than the temperature range for the formation of monolayer BP (600–850 K). This implied that compared to monolayer BP, the growth conditions for bilayer BP were more sensitive to temperature. After the formation of the bilayer BP, where the two sheets of boron were stacked over one another through interlayer boron–boron covalent bonding, each sheet had a β_{12}-like structure with zig-zag rows of boron atoms on the entire Cu(111) surface. Further deposition of boron atoms led to the development of 3D boron clusters instead of the thickening of the BP layers. A large charge transfer and redistribution took place between the first boron layer and the Cu (111) substrate, which facilitated extra electrons for the bonding of additional boron atoms on the first layer, making the formation of the second layer of boron possible. The bilayer BP displayed a metallic character and had a less tendency to get oxidized than its monolayer analogue.

Segregation-enhanced epitaxy (SEE)

SEE is a promising alternative to MBE for the fabrication 2D materials such as BP. Hoegen's group[47] developed stable (6 × 2) reconstructed BP χ_6-polymorph using this technique. The BP was grown on a cleaned Ir(111) substrate (99.99% purity), and purified borazine ($B_3H_6N_3$) was used as the precursor. At a high-temperature range of 1123–1373 K and a pressure of 5×10^{-8} mbar, the borazine dosed on the surface of Ir(111) resulted in the formation of h-BN and BP layers on the substrate surface. At high dosing temperatures, borazine decomposes and results in the deposition of B with the desorption of N over the substrate. The synthesized BP displays metallic characteristics with a V-shaped decrease in the density of states at the Fermi level, which suggests its Dirac-like behavior.

van der Waals epitaxy (vdWE)

Wu *et al.*[48] successfully constructed a large-scale BP sheet on a mica substrate *via* van der Waals epitaxy. Sodium borohydride ($NaBH_4$) powder was used as the boron source and to ensure the quality before the growth process, wherein $NaBH_4$ was annealed at 763 K for 2 h. The synthesis was carried out in two zones inside the tube furnace where freshly cleaved fluorophlogopite mica ($KMg_3AlSi_3O_{10}F_2$) was used as the substrate. Based on the first-principles calculations, it was predicted that the as-synthesised BP structure matched well with the α′ 2H-BP. The thickness of the synthesized BP layer was *ca.* 1.7 nm, and partial hydrogenation stabilized its structure. The material served as a good high-performance photodetector.

Top-down synthesis of borophene

Liquid phase exfoliation (LPE)

CVD and PVD methods for the syntheses of borophenes need extreme conditions that are very expensive to maintain, such as ultra-high vacuum or high temperature, and involve complex chemistry. Thus, slow growth rate and high cost of production limit the application of these methods in industry. These constraints have led researchers to focus on alternative cost-effective and simple methods for the synthesis of high-quality BP.

Li *et al.*[49] developed high-quality few-layer boron sheets by an ultrasound-assisted liquid-phase exfoliation process (Fig. 5A–D). In this process, boron powder (95%, with an average particle size of 2 μm) was taken as the boron source and it was exfoliated by high-power probe-type sonication (350 W for 4 h). By varying the solvent in the exfoliation process and controlling the centrifugation speeds, it was possible to control and tune the lateral size and thickness of the exfoliated B sheets. Using DMF (dimethyl formamide) and IPA (isopropyl alcohol) as exfoliating solvents, the average area of the boron sheets obtained was 19 827 nm^2 and 1791 nm^2, whereas the average thickness was measured to be 1.8 and 4.7 nm, respectively. The dispersion of the as-prepared few-layer B sheet had high solubility in DMF (up to 1.16 mg mL^{-1}) and was stable under ambient conditions for at least 50 days. These few-layer boron sheets were applied as supercapacitor electrode materials, and the prepared device delivered a potential window as high as 3.0 V.

Ji and coworkers[50] designed a novel top-down method by combining liquid exfoliation with thermal oxidation and etching to produce large quantities of superior ultrathin 2D boron nanosheets. In this method, at first, bulk boron powder was exfoliated into thick layers using a sonication process in a solvent mixture of NMP (*N*-methyl-2-pyrrolidone) and ethanol (1 : 1 v/v). Then, the exfoliated layers were oxidized in oxygen at 923 K to form B_2O_3, which on subsequent liquid phase exfoliation produced the boron nanosheets. The planar size and thickness of these as-prepared boron nanosheets were *ca.* 100 nm and <5 nm, respectively. The biocompatibility and dispersibility of the sheets were improved by modifying them

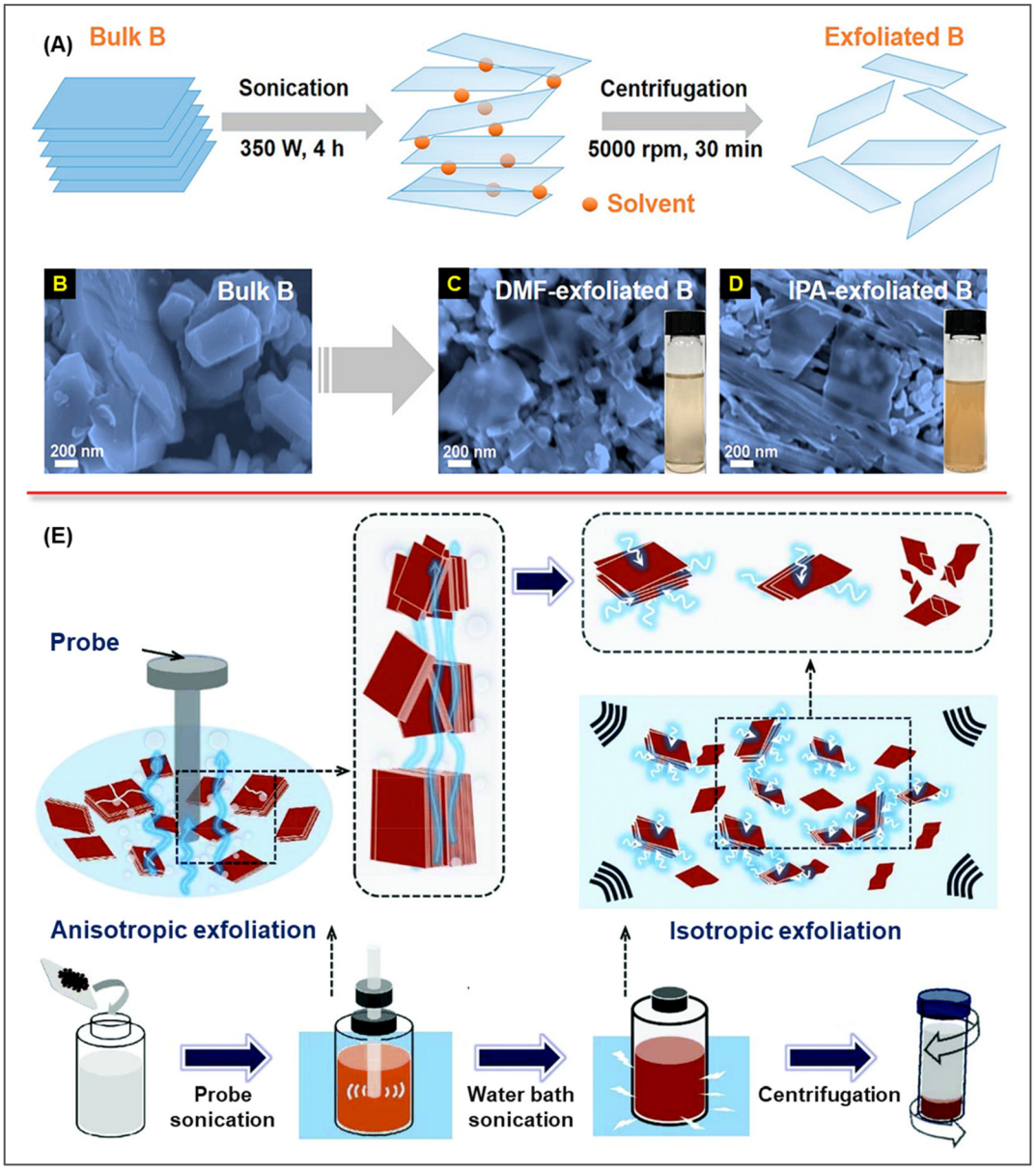

Fig. 5 Synthesis of borophene sheets by different LPE processes. (A) Ultrasound-assisted LPE process in DMF/IPA solvent, (B) SEM images of bulk boron and boron sheets obtained in (C) DMF and (D) IPA solvent. Reproduced with permission. Copyright 2018, American Chemical Society.[49] (E) 2D ultrathin boron nanosheets with the expected morphological evolution process. Reproduced with permission. Copyright 2020, The Royal Society of Chemistry.[51]

with positively charged amine-functionalized polyethylene glycol (PEG-NH_2) through electrostatic adsorption.

The group of Zhang and Zhang[51] demonstrated how to effectively develop highly crystalline 2D boron nanosheets using a liquid phase exfoliation method (Fig. 5E). Bulk boron powder was subjected to high power sonication (600 W for 1 h and 750 W for 2 h) in isopropyl alcohol as the exfoliating solvent at a fixed temperature of 283 K, followed by high-speed centrifugation. The study showed the effect of centrifugation speed on the thickness of the as-prepared multilayered boron nanosheets. When the centrifugation speed was 3000–6000 rpm, 6000–9000 rpm and 9000–12 000 rpm, the average thicknesses of the few-layered boron sheets were reported to be 20.0 nm, 4.8 nm and 1.9 nm, respectively, and the thickness of each single atomic layer was 0.3 nm. The optoelectronic properties of these 2D nanosheets of boron have been explored in photoelectrochemical (PEC) and field-effect transistor (FET)-type photodetectors.

Guo and coworkers[52] successfully fabricated ultrathin 2D borophene nanosheets (thickness <2 nm) by sonication-assisted liquid exfoliation. They took crystalline boron flakes as the boron source in ethanol and ultrasonicated the dis-

persion at a power of 2000 W for 24 h. The presence of the β-rhombohedral phase of BP was confirmed in the as-synthesized product from HR-TEM (high resolution-transmission electron microscopy) analysis and the β_{12} phase of BP from Raman spectroscopy. The thickness of the randomly selected 2D borophene nanosheets ranged between 1.32 and 1.87 nm.

John's group[53] reported the surfactant-assisted liquid-phase exfoliation of BP layers from boron and subsequently refined them into the β rhombohedral structure. Poly(ethylene glycol) (PEG) polymeric chains with neutral characteristics were simultaneously introduced with cationic surfactants such as cetyltrimethylammonium bromide (CTAB) and anionic surfactants such as sodium dodecyl sulfate (SDS) to produce a β rhombohedral crystal structure in the BP layers by constructive engineering. Raman and HR-TEM analyses indicated the presence of β_{12}, χ_3 and γ orthorhombic phases in the polymer-induced crystal structure-engineered BP. By observing the electrocatalytic hydrogen evolution reaction (HER) performance of the BP, it was suggested that the neutral polymeric chains of PEG act as better exfoliating agents in comparison to ionic surfactants, namely, CTAB and SDS.

Li *et al.*[54] synthesized sulfur and iron-doped BP. The β_{12} borophene was developed by the exfoliation of boron powder in NMP solvent under ultrasonication (40 kHz, 72 h). Then, the synthesized β_{12} borophene was doped separately by sulfur powder and $FeCl_3$ through microwave treatment, leading to the respective doped samples. From the AFM study, the thickness of the as-prepared pure BP was found to be *ca.* 1.6 nm, whereas for the sulfur and iron-doped BP, it was *ca.* 2 and 10 nm, respectively.

Mechanical exfoliation (ME)

Chahal *et al.*[55] produced mono- and few-layered BP sheets *via* cost-effective micromechanical exfoliation (Fig. 6A–D). It was demonstrated that the exfoliation of BP into atomic sheets can successfully be done using double-sided foam tape (with viscous adhesive polymer) having strong adhesive force and capable of exerting the necessary force for exfoliation. From the HR-TEM imaging and Raman spectroscopy, it was identified that the β_{12} and χ_3 phases were predominantly produced. The widths of the exfoliated sheets were found to be 5, 9, 13, 21 and 41 Å, which correspond to the formation of monolayer, bilayer, trilayer, 5 layers and 10 layers of BP, respectively.

Zielinkiewicz and coworkers[56] reported the fabrication of few-layered BP by a ball-milling process where they varied the operational parameters such as the initial mass loading of bulk boron (1.0, 2.0 and 3.0 g), rotation speed (250, 450 and 650 rpm) and ball-milling time (1, 3, 6 and 12 h). The conditions were optimized to 1.0 g of bulk boron loading with a rotation speed of 450 rpm and ball-milling time of 6 h, which resulted in the construction of thin and uniform few-layered BP flakes with a thickness of *ca.* 5.5 nm. When higher mechanical energy is applied during ball-milling, the resultant BP forms a different crystalline phase due to the internal heat produced, which affects the structure of BP. It was further observed that the ball-milling process gives rise to the formation of new crystal phases of BP, and the results indicated the presence of β-rhombohedral, γ-orthorhombic and τ-B phases. Subsequently, a sustainable and scalable construction route was put forward by the same group[57] using a combination of ball-milling and ultrasound-assisted liquid phase exfoliation process with biocompatible intercalants (sodium cholate, urea and sodium chloride) in aqueous media (Fig. 6E). It was established that sodium cholate was the most efficient intercalant and an optimized ball-milling condition of 450 rpm for 6 h produced 4-layer BP. Further, tuneable 3-layer BP sheets could be achieved by a combination of ball-milling and ultrasound-assisted liquid phase exfoliation techniques. The long-term oxidation resistance of these 3- and 4-layered BP samples in the presence of air was also demonstrated.

Electrochemical exfoliation (ECE)

The group of Mijowska[58] demonstrated the electrochemical exfoliation of bulk boron to few-layered BP (Fig. 6F). This unique effect was achieved by adding bulk boron to Cu/Ni metal mesh, which induced electrical conductivity and created a pathway for the production of BP flakes with a thickness of *ca.* 3–6 nm having different phases. The syntheses were carried out in two different electrolytic media, one was LiCl in dimethyl sulphoxide (DMSO) and another was Na_2SO_4 in deionized water (DI). The sample developed on Cu-mesh matched with the β-rhombohedral boron structure whereas the one produced using Ni-mesh was in line with the theoretical predictions for β_{12} and χ_3 lattice parameters.

Chowdhury *et al.*[59] developed an innovative method for the synthesis of BP based on the idea of graphene synthesis by electrochemical exfoliation process where platinum was chosen as the anode and boron acted as the cathode material. With an increase in the temperature, the conductivity of the boron-attached heating coil increased, which confirmed the formation of BP from boron. This approach also monitored the quality and crystallographic structure of the anisotropic BP sheets as a function of temperature. The developed BP having a zeta potential value greater than +100 mV indicated the excellent stability of the material. The size of the BP sheets was found to be between 400 and 600 nm.

Modified Hummers' method

Freestanding BP with monolayer as well as sheets with few layers were experimentally prepared for the first time by Kumar and Vinu.[60] Large-scale freestanding pure crystalline BP synthesis was introduced *via* a combination of sonochemical liquid phase exfoliation technique and modified Hummers' method. The presence of β_{12}, χ_3 and their intermediate phases of BP in the as-prepared samples was confirmed by electron microscopy study. The constructed few-layer BP sheets had a lateral dimension of 20–100 nm with an interplanar distance of 2.6 Å. The metallic nature of the synthesized BP sheets was established by STM analysis, which agreed well with DFT (density functional theory) band structure calculations. The freestanding BP was studied for its applications in

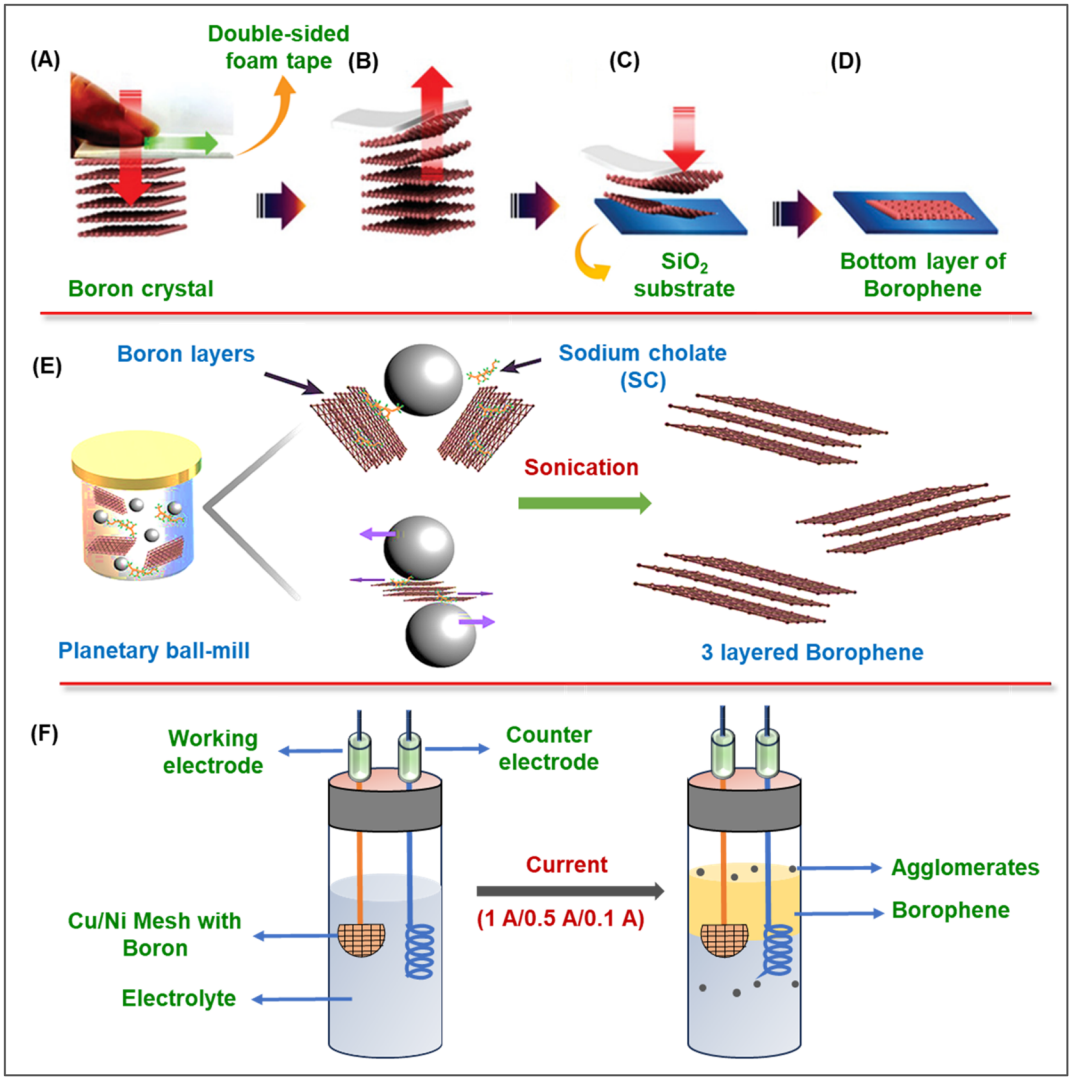

Fig. 6 Synthesis of borophene sheets by ME and ECE methods. (A) Double-sided foam tape-assisted exfoliation of the boron layers through normal (red arrow) and shear (green arrow) forces, (B) peeling off the layers from a crystal, (C) exfoliated layers pressed against the substrate and (D) transfer of bottom layer of exfoliated borophene to the substrate. Reproduced with permission. Copyright 2021, Wiley-VCH GmbH.[55] (E) Borophene flakes *via* ball-milling with intercalants and ultrasound assisted-LPE. Reproduced with permission. Copyright 2024, Elsevier B.V.[57] (F) Electrochemical exfoliation of boron.[58]

gas, photo, strain and surface-enhanced Raman scattering (SERS)-based molecular sensing.

Joshi *et al.*[61] synthesized oxidized BP sheets by the oxidative exfoliation of boron into thin layers in the presence of potassium permanganate in an aqueous solution. The presence of the β-rhombohedral phase of BP was concluded from the XRD pattern while the other two, namely, the β-phase and oxidized β-phase, were confirmed by Raman analysis. This oxidative exfoliation technique afforded BP with few layers (~8.5 nm thicknesses), as evident from AFM imaging, which maximized the electroactive surface area and also added stability to the structure in aqueous electrolytes. The BP, thus developed, showed high conductivity (96.12 S m^{-1}), good rate capability (>59%) and excellent cycling stability (>80%).

Thus, it may be inferred that in both bottom-up and top-down synthesis processes, there are different types of limitations. The CVD and PVD synthetic methods have the advantage of producing highly pure, stable monolayer structures of BP with good crystallinity and uniform thicknesses. But these processes are very slow, expensive, highly complicated and require highly controlled conditions such as ultra-high vacuum and high temperature. The choice of an appropriate substrate material is also crucial for proper deposition or epitaxial growth in the synthesis of individual structures of BP. On the other hand, different exfoliation techniques such as liquid phase exfoliation, mechanical exfoliation, and electrochemical exfoliation are simpler and relatively cost-effective, with the added advantage of scalability to achieve free-stand-

ing BP sheets. However, the quality of the structures is not as pure as that obtained from CVD or PVD and it is also difficult to maintain the size and thickness of the as-prepared borophenes. Generally, these methods give a mixture of different phases of low-quality few-layer BP but they are more eco-friendly than CVD or PVD techniques. In the modified Hummers' method, monolayers of freestanding borophenes as well as few-layer BP sheets have been experimentally synthesized with scalability, but it poses the risk of oxidation. Thus, there is still a lot of scope to develop effective synthetic strategies of BP, which will ensure the scalability of the product without compromising on its quality as well as precise control of the structures, purity, crystallinity, size and thickness.

Unique properties of borophene

Mechanical properties

In the application of flexible electronic devices, sensors and various nanoscale mechanical systems, flexibility is essential, where the material must be able to tolerate strain and repetitive deformations. The anisotropic mechanical properties of BP are more interesting due to the presence of strong B–B bonds and unique structural characteristics. The mechanical properties in BP change along the zig-zag direction and armchair direction due to its anisotropic nature. In the zig-zag direction, the boron atoms are arranged in a staggered pattern, whereas in the armchair direction, atoms are in a linear orientation. The network of hollow hexagons (HHs) in the structure has a profound impact on the tensile strength of BP.[62] By the judicial adjustment of the atomic structure and lattice symmetry of the BP sheet, researchers have been able to modify its mechanical properties. This makes provision for customising the mechanical strength and flexibility, which is an important parameter for certain specific applications. The ability of BP to conform to different shapes and surfaces improves their freedom of design in flexible electronic devices with irregular or curved surfaces. In contrast to other two-dimensional materials, BP shows strain-induced structural phase changes and a negative out-of-plane Poisson's ratio, which leads to exceptionally high ductility but low breaking strains. When the strain is increased, the boron atoms rearrange themselves in an auxetic pattern, which further strengthens the BP sheet. The presence of HHs in the structure influences the ductility of BP.[63] The mechanical properties of 2D borophene sheets were studied by first-principles calculations. Specifically, a BP sheet with a hollow hexagon's concentration of 1/6 has a bending stiffness four times lower than that of graphene, which is attributed to the presence of HH rows that are spaced optimally.[20] These BP sheets have been shown to possess an in-plane modulus (C) of 210 N m^{-1} and bending stiffness (D) as low as 0.39 eV, reaching their Foppl–von Karman number per unit area (C/D) of 568/nm^2. This value is more than two-fold higher than that of graphene, which makes BP a material that bends and crumples more easily than it stretches and thus establishes BP as one of the most flexible materials. The strong in-plane elasticity of BP, aided further by its low mass density, leads to a specific modulus of 346 m^2 s^{-2}, which is comparable to the value of graphene. Even more surprising is the fact that the ideal strength of the BP sheet is 16 N m^{-1}, which is several times higher than that of MoS_2 monolayer, phosphorene and silicene and only second to hexagonal boron nitride and graphene.[62] Wang *et al.* estimated that the Young's modulus of BP is 378.97 and 162.49 N m^{-1} along the x- and y-axis, respectively. When BP is hydrogenated (borophane), the values are reduced to 172.24 and 110.59 N m^{-1}, respectively.[64] This can be attributed to the fact that after hydrogenation, the B–B bond gets elongated and the bond strength decreases; consequently, the values of Young's modulus decrease. The Young's modulus and shear modulus of the α sheet, β_{12} and χ_3 2D boron phases are not strongly direction-dependent, but the Young's modulus of the *Pmmn* 2D boron phases are very anisotropic.

Thermal conductivity

Borophene has remarkable thermal characteristics, which include both thermal conductivity and thermal stability. In this process, a complicated phonon transport and scattering mechanism is involved, which arises from its structural anisotropy. Sun *et al.*[65] investigated the thermal properties of BP using the first-principles. According to their study, along the armchair direction of BP, the Young's modulus is similar to that of graphene, however, the thermal conductivity is only a few percent compared to graphene, attributed to the strong phonon–phonon scattering. The lattice thermal conductivity of the material can be considerably decreased when the characteristic lengths of BP sheets are smaller than 300 to 400 nm along the armchair and zig-zag directions.[65] Zhou *et al.*,[66] through first-principles calculations and non-equilibrium Green's function (NEGF) technique, examined BP's lattice thermal transport characteristics both for the β_{12} and hexagonal models. In the hexagonal model, the lowest thermal conductance is 62% of the highest one, while the same is only 30% in the β_{12} model at room temperature. This suggests the highly anisotropic thermal conductivity characteristic of BP. Interestingly, at room temperature, the maximum thermal conductance reaches 7.87 nW (K nm^2)$^{-1}$ and 10.97 nW (K nm^2)$^{-1}$ for hexagonal and β_{12} phases, respectively, which are higher than that of graphene. The thermal conductivity predicted using the molecular dynamics method shows an increase in its value with an increase in the sample length. However, as the length becomes infinite, the thermal conductivity of BP becomes greatly inhibited due to its buckling. This increases the out-of-plane phonon scattering and leads to significant diffusion thermal transport.[67] Using first-principles calculations and the Boltzmann transport equation, it has been predicted that the lattice thermal conductivity of α-sheet of BP[68] is isotropic along the armchair direction, and its value at room temperature has been estimated to be 14.34 W K^{-1} m^{-1}.[69] Significantly, other studies reported the higher anisotropic thermal conductivity of the 2-*Pmmn* phase of BP, and

its value has been calculated to be *ca.* 147 and 76 W K^{-1} m^{-1} along the armchair and zig-zag directions, respectively.[70] Hydrogenated BP has greater thermal conductivity than pristine BP, suggesting the higher contribution of electrons towards the conductivity than the phonons.[71] The thermal conductivity may be enhanced by the intercalation of metal atoms in BP. For example, the thermal conductivities of the δ_4 sheet along the armchair and zig-zag directions are 53.8 and 115.7 W K^{-1} m^{-1}, respectively, at 300 K. On the other hand, the thermal conductivity of AlB_6 along the armchair and zig-zag directions increases to 160.2 and 157.2 W K^{-1} m^{-1}, respectively. To summarize, the thermal conductivity of BP decreases with an increase in temperature, increases with an increase in length and displays an anisotropic increase.

Electronic property

Many studies have been conducted on the electrical properties of BP, revealing its fascinating characteristics and prospective uses, especially in the field of energy storage technology. Borophene, a single-layer material with an anisotropic atomic structure, massless charge carriers (Dirac fermions) and the ability to tailor its bandgap, offers novel electronic properties that are useful in optoelectronics and other electronic devices. The exceptional charge carrier mobility and high thermal conductivity of BP arise from the presence of Dirac fermions.[29] The 2-*Pmmn*, β_{12} and χ_3 phases of BP show metallic behavior. Typically, the 2-*Pmmn* BP is metallic but to be more specific, this phase shows anisotropy in its electronic structure with a metallic nature along the armchair direction while along the zig-zag direction, a semiconducting nature is observed with a bandgap.[72] One of the most fascinating features of BP is the capability to engineer its bandgap through different methods, thereby manoeuvring its behaviour from metallic to semiconducting. Some of these methods include strain/defect engineering and chemical treatment of the surface of BP, and the resulting energy gap depends on the functional groups utilized.[73] The introduction of oxygen defect sites may generate significant scattering, leading to a decrease in the electronic conductivity and carrier mobility of the oxidized BP. The band gap varies with the amount of O doping; after 25% doping, BP shows an increased bandgap of 0.22 eV, whereas after 50% doping, the bandgap reduces to zero compared to pure BP. This implies that after the introduction of 25% O defect, the character of doped BP shifts from metallic to p-type semiconductor and on 50% O doping, a semimetallic character evolves.[74] It is interesting to note that when subjected to uniaxial/biaxial tensile or compressive strains, the metallic BP starts exhibiting a semiconducting character. On applying 6% strain, the β_{12} borophene displays an isotropic semiconducting nature with a bandgap of 0.7 eV, whereas χ borophene shows an anisotropic semiconducting feature with 0.6 and 1.2 eV bandgap along the zig-zag and armchair directions, respectively.[27] This study suggests that by the introduction of strain, it may be possible to alter the metallic character of BP. Another way to change the metallic nature to a semimetallic or semiconducting character is by the chemical functionalisation of the surface of BP (hydrogenated or fluorinated BP) with a Dirac cone at the Fermi level between the Y and Γ point. Fully fluorinated borophenes are unstable. The 2 *Pmmn* phase shows little tendency to form B_4F and B_2F, among which B_4F retains the metallic character whereas B_2F is semiconducting with a bandgap of 0.4 eV.[75] On the other hand, after the hydrogenation of β_{12} BP, the superconducting property significantly improves. In addition to that, the application of tensile strain (up to 5%) and hole doping significantly enhance the critical temperature (T_C) of superconductivity, which reaches up to 28.6 K. This is higher than the liquid hydrogen temperature (20.3 K) and thus enhances its practical applications in various fields. Both the B-σ and B-p_z states of the Fermi level are crucial for this superconductivity.[76] For the application of BP in electronics, a fascinating issue is the localization of the mobile electrons of BP and ultimately the opening of its band gap. The quantum confinement induced by the fabrication of finite-sized structures, such as ribbons, dots and edges, is one of the significant approaches to achieve band gap tuneability.[75] 1D-BP nanoribbon strips exhibit quantum-confined electronic properties, which are absent in the extended 2D-BP sheets. The electronic properties of single-phase $v_{1/6}$ and $v_{1/5}$ BP nanoribbons are dominated by Friedel oscillations and striped moiré patterns, respectively. On the other hand, mixed-phase BP nanoribbons exhibit quantum-confined states with an increase in the number of nodes in the electronic density of states at higher biases. Thus, the high degree of polymorphism as well as diverse edge topologies in BP nanoribbons offer a rich quantum platform for the study of 1D-electronic states.[77]

Other properties

Detailed studies on the photoelectric properties of α-sheet of BP doped with Al and Ga using the first-principles pseudopotential plane wave method suggest an increase in the static dielectric constant of doped BP from 2.60 to 3.21 for Al doping and 3.57 for Ga doping with the appearance of new dielectric peaks, which indicate that doping can enhance the electromagnetic energy storage ability of BP. After doping, the reflectivity of BP decreases and the static refractive index shifts from 1.61 to 1.79 for Al and 1.89 for Ga. Simultaneously, the doped BP system bridges the gap between red light and infrared absorption. These research outcomes reveal that BP-based systems may be used in infrared detection devices.[78] Further, it is possible to tune the magnetic and electronic properties of BP by doping certain 3d transition metals. It has been shown that the doping of only Cr and Mn on β_{12} and χ_3 borophene shows magnetic properties, whereas the other 3d transition metals show no effect on the magnetic behavior.[79] Borophene, belonging to the family of 2D Dirac materials, is also anticipated to show superconductivity properties by virtue of its low mass with a strong electron–phonon coupling. The hexagonal molecular geometry of BP with various critical temperatures promotes the superconducting properties.[80]

Potential application of borophene in supercapacitors

What are supercapacitors?

Energy storage systems are an inevitable part of the utilization of renewable energy as their sources are discontinuous in nature; hence, the energy derived from them is required to be stored for future use. Thus, energy storage technologies are one of the best alternatives to cope up with the progressively growing demand for energy.[81] In this regard, supercapacitors have attracted considerable interest due to their high power density, rapid charge/discharge, excellent cycling stability and consistent energy density, which links the gap between capacitors and batteries.[82,83] Simple physical capacitors are usually made up of two parallel plates, one positively and another negatively charged, separated by an insulating dielectric sheet where the charge is stored in the form of an electric potential energy between the two plates (Fig. 7A). In supercapacitors or ultracapacitors, the electrodes are separated by an ion-permeable separator with a suitable electrolyte (Fig. 7B).

Charge storage mechanism of supercapacitors

The charge storage mechanism of supercapacitors is of two types, one is the electrical double layer capacitance (EDLC) and the other is pseudocapacitance (involving faradaic charge transfer through redox reactions). Pure EDLC systems are associated only with electrostatic separation of charges on the electrical double layer formed at the interface of the electrode/electrolyte (Fig. 7C).[84] When potential is applied, the ions of the electrolyte migrate and get adsorbed on the surface of the electrode to form a double layer of charges. Carbon materials such as activated porous carbons, carbon nanotubes, and graphene show their charge storage properties predominantly through EDLC. On the other hand, pseudocapacitance is associated with rapid and reversible faradaic redox reaction on the surface of the electrode (Fig. 7D). The energy density in pseudocapacitors is higher than EDLC but the cyclic stability of EDLCs is higher than that of the pseudocapacitors. Metals, metal oxides, metal sulphides, conducting polymers, heteroatom-doped carbons, *etc.*, are responsible for showing pseudocapacitive properties. In a hybrid supercapacitor, both EDLC and faradaic pseudocapacitance mechanisms operate (Fig. 7E) and hence energy density as well as power density are high compared to traditional EDLCs and pseudocapacitors. In this type of supercapacitor, one electrode is made up of a pure carbon-based material, which gives EDLC, and the other electrode usually consists of metal or conducting polymer-based material, which contributes to pseudocapacitance in the total capacitance.[85] In the functioning of the supercapacitor, the electrolyte plays an important role, and its judicious choice for each individual electrode material is also crucial. The electrolyte must be stable and should resist degradation of the cell within the potential window chosen for the study. Different types of electrolytes are available to solve the purpose, which includes aqueous (H_2SO_4, KOH, Na_2SO_4, *etc.*), organic (tetraethylammonium tetrafluoroborate/acetonitrile, 1-butyl-3-methylimidazolium tetrafluoroborate, *etc.*) and solid-state (gel

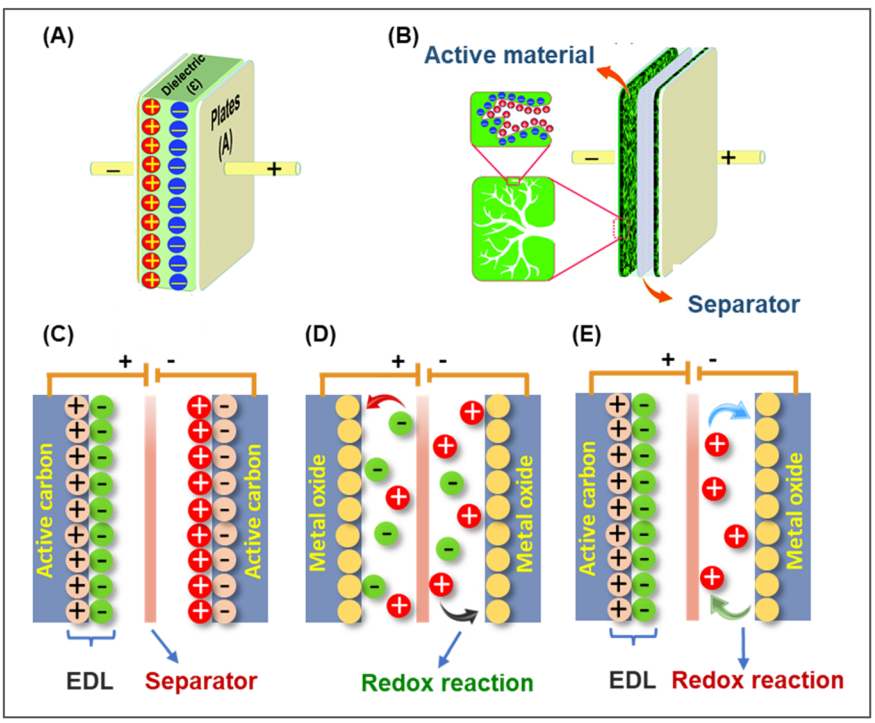

Fig. 7 Schematic representation of (A) conventional capacitor and (B) supercapacitor. The energy storage mechanism of (C) EDLC, (D) pseudocapacitor and (E) hybrid supercapacitor. Reproduced with permission. Copyright 2019, The Royal Society of Chemistry.[84]

polymer of polyvinyl alcohol/H_2SO_4, poly(methyl methacrylate) solid polymer, *etc.*) electrolytes.[86,87] The specific capacitance values are calculated from cyclic voltammetry (CV) and galvanostatic charge/discharge (GCD) studies using eqn (i) and (ii), respectively.[88]

$$C_s = \frac{\int_{v_i}^{v_f} I(v)\mathrm{d}v}{(v_f - v_I) \times S \times m} \quad \text{(i)}$$

Herein, C_s denotes the specific capacitance in F g^{-1}, ' $\int_{v_i}^{v_f} I(v)\mathrm{d}v$ ' is the area under the corresponding cyclic voltammogram, '$(v_f - v_i)$' is the potential window in V, 'S' is the scan rate in V s^{-1} and 'm' is the mass of the active electrode material in g.

$$C_s = \frac{I \int v\mathrm{d}t}{m \times (v_f - v_I)} \quad \text{(ii)}$$

Here, 'I' is the discharge current in A, ' $\int v\mathrm{d}t$ ' is the area under the discharge curve, 'm' is the mass of the active electrode material in g and '$(v_f - v_i)$' is the potential window in V.

Applications

Borophene is a very promising electrode material for energy storage systems such as batteries and supercapacitors since it is a 2D material with better electrochemical properties than graphene. It shows a large and stable voltage window, excellent specific capacitance (theoretical capacitance: 400 F g^{-1}, four times of graphene),[32] good rate capability and recyclability.[37] Depending on the desired application, BP can be engineered to act as energy storage systems, transistors, sensors and other electronic devices. BP has remarkable features such as tuneable energy bandgap, excellent electronic conductivity, lightweight, high specific surface area, high chemical stability and low diffusion barriers, which makes it a potential candidate for applications in supercapacitors. Moreover, BP has excellent mechanical properties, including high flexibility and strength, which make it possible to design flexible and wearable supercapacitors. The performance of various BP-based materials in supercapacitors has been summarized in Table 2.

In 2018, Li *et al.*[49] fabricated a symmetric supercapacitor using DMF-exfoliated layered boron nanosheet with ionic liquid 1-butyl-3-methylimidazolium hexafluorophosphate as an electrolyte (Fig. 8A–F). The prepared cell operated in a high potential window range (3.0 V) and showed nearly rectangular cyclic voltammograms even at a high scan rate of 100 mV s^{-1}, which indicated its extraordinary capacitive behaviour. From GCD measurements, the highest specific capacitance calculated at a current density of 0.3 A g^{-1} was 147.6 F g^{-1}, which was greater than that of bulk boron (41.7 F g^{-1}). From the Ragone plot, the energy density was found to be as high as 46.1 W h kg^{-1} at a power density of 478.5 W kg^{-1}. The material exhibited remarkable cycling stability, retaining 88.7% of the initial specific capacitance after 6000 cycles. The device fabricated with the material could illuminate a red LED light and run a mini-fan after charging for a few seconds.

Joshi *et al.*[61] engineered oxygen defect in the β-rhombohedral phase of BP (few layers thickness ~8.5 nm) and explored its electrochemical property (Fig. 8G–I). In this approach, oxidative exfoliation was employed to maximize the electroactive surface area and also to stabilize the structure in aqueous electrolytes. The as-prepared sample with a planar 2D structure had high conductivity (96.12 S m^{-1}), which led to its high ion diffusion rate in aqueous electrolytes. Boron nanosheets with O-defects showed relatively better pseudocapacitive performance in basic (KOH) and acidic (H_2SO_4) media than in neutral (Na_2SO_4) electrolytic medium. In KOH and H_2SO_4 media, the material exhibited comparable charge storage capability at high current densities, while at low

Table 2 Summary of performance of borophene-based materials in supercapacitors

Entry	Material	Electrolyte	Potential window (V)	Capacitance (current density/ scan rate)	Energy density (W h kg^{-1})/power density (W kg^{-1})	Capacitance retention (%)/ cycle number	Ref.
1	Boron nanosheets (symmetric supercapacitor, SSC)	[bmim][PF_6]	0 to 3.0	147.6 F g^{-1} (0.3 A g^{-1})	46.1/478.5	(88.7%/6000)	49
2	O-defective boron nanosheets (three electrode system)	H_2SO_4	0 to 0.8	141.55 mF cm^{-2} (2 A g^{-1})	—	(84.7/5000)	61
	O-defective boron nanosheets (SSC)	[bmim][BF_4]	0 to 3.0	22.24 F g^{-1} (1 A g^{-1})	25.1/636.13	(75.4%/8000)	
3	PANI: α borophene (three electrode system)	1 M H_2SO_4	−0.3 to 1.2	960 F g^{-1} (10 mV s^{-1})	—	(95%/1000)	36
4	(PEDOT: PSS)/β_{12} borophene (three electrode system)	H_3PO_4/PVA	−0.8 to 0.8	853 F g^{-1} (2 mV s^{-1})	—	(95%/1000)	35
5	Borophene coated graphoil (three electrode system)	1 M H_2SO_4	0 to 0.8	350 mF cm^{-2} (1 A g^{-1})	—	—	42
6	SNC-borophene (three electrode system)	3 M KOH	−1.0 to 0	607 F g^{-1} (1 A g^{-1})	—	(91.7/1000)	89
	SNC-Borophene (SSC)	PVA/KOH	0 to 1.4	230.7 F g^{-1} (1 A g^{-1})	29.2/3500	(90.67%/5000)	
7	Fe-borophene	6 M KOH	0 to 0.45	202 F g^{-1} (0.25 A g^{-1})	—	(61.1%/5000)	54
	S-Borophene (three electrode system)		0 to 0.48	120 F g^{-1} (0.25 A g^{-1})		(100.5%/5000)	
8	MxB (50 : 50) (three electrode system)	2.0 M H_2SO_4	−0.7 to 0.5	626.7 F g^{-1} at 1 A g^{-1}	—	(88.5%/10 000)	34
	MxB (50 : 50) (SSC)	PVA/H_2SO_4	0 to 1.2	375 F g^{-1} at 1 A g^{-1}	75.6/600	(93.6%/10 000)	

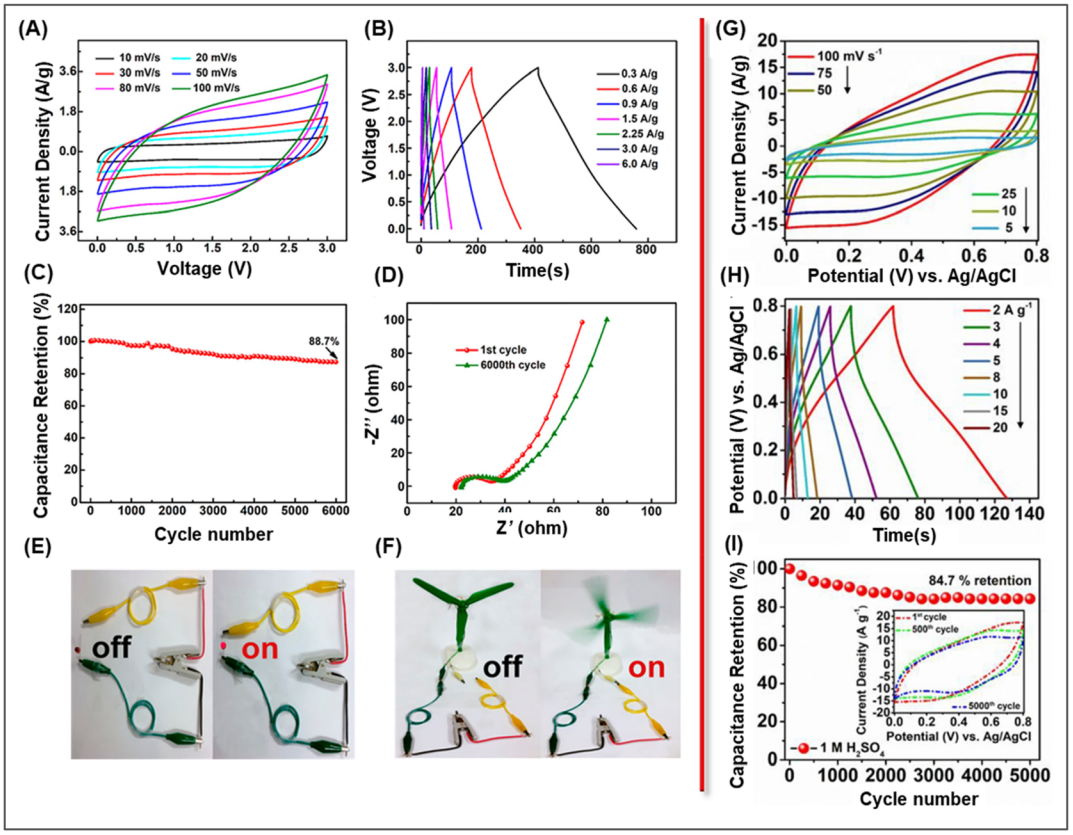

Fig. 8 (A–F) Electrochemical performance of DMF-exfoliated few-layer B sheet-based supercapacitor in ionic liquid electrolyte. (A) CV curves at various scan rates, (B) galvanostatic charge/discharge curves at different current densities, (C) recyclability at a scan rate of 50 mV s^{-1} for 6000 cycles, (D) Nyquist plots before and after 6000 cycles and photographs of the obtained coin cell operating (E) a red LED light and (F) a mini-fan. Reproduced with permission. Copyright 2018, American Chemical Society.[49] (G–I) Electrochemical performance of O-defective boron nanosheets in 1 M H_2SO_4 electrolyte. (G) CV curves at various scan rates, (H) GCD curves at different current densities and (I) recyclability at a scan rate of 100 mV s^{-1} for 5000 cycles. Reproduced with permission. Copyright 2020, Elsevier B.V.[61]

current density, it showed high charge storage in H_2SO_4 electrolyte. In a three-electrode system, this oxygen-defective boron nanosheet gave a capacitance value of 107.63 mF cm^{-2} with a relaxation time of 0.83 s and 141.55 mF cm^{-2} with a relaxation time of 1.78 s at a current density of 2 A g^{-1}, in KOH and H_2SO_4, respectively. A symmetric cell constructed with high potential window (3.0 V) in ionic liquid electrolyte [bmim][BF_4] (1-butyl-3-methylimidazolium tetrafluoroborate) retained 75.4% of its initial capacitance after 8000 CV cycles at a high scan rate of 300 mV s^{-1} with high specific energy of 25.1 W h kg^{-1} and specific power of 636.13 W kg^{-1}.

Taşaltın *et al.*[36] developed a nanocomposite of crystalline α-borophene and polyaniline (PANI) over flexible Ni foam substrate as a promising electrode material for supercapacitors. The zeta potential studies showed that α-borophene had sufficient electrostatic repulsion, imparting good physical stability to the structure. CV studies performed in 1 M H_2SO_4 electrolyte (potential window −0.3 V to 1.2 V) revealed that the calculated specific capacitance values of the prepared α-borophene, PANI and PANI: α-borophene electrodes were 486, 385 and 960 F g^{-1}, respectively. The capacitance retention in the PANI: α borophene electrode was found to be 95% after 1000 cycles, implying no significant degradation in the specific capacitance of the electrode.

Türkmen and coworkers[35] explored the electrochemical performance of an inorganic–organic hybrid nanocomposite of poly(3,4-ethylenedioxythiophene):polystyrene sulfonate (PEDOT:PSS)/β_{12} borophene using ionically crosslinked conducting polymer PEDOT:PSS with a uniform distribution of the β_{12} phase of BP. The synthesized BP film and PEDOT:PSS film showed electrical conductivities of 14×10^{-6} and 752 S cm^{-1}, respectively. CV measurements in H_3PO_4/PVA gel electrolyte at 2 mV s^{-1} gave specific capacitance values of 230, 622 and 853 F g^{-1} for the PEDOT:PSS, PEDOT:PSS/BP (75/25, wt%) and PEDOT:PSS/BP (50/50, wt%) electrodes, respectively. The PEDOT:PSS/BP (50/50, wt%) electrode retained 95% of its initial capacitance value after 1000 cycles.

Abdi *et al.*[42] fabricated nanosupercapacitors by depositing 2D-borophene sheets on graphoil (a soft sheet form of compressed natural graphite) through a wet-transfer method. The electrochemical measurement for supercapacitor application was carried out in 1 M H_2SO_4 in a three-electrode system. Using this working electrode, the CV study at a scan rate of 5 mV s^{-1} in the potential window of 0–1 V showed a specific

capacitance of 270 mF cm^{-2}, whereas the calculated specific capacitance from the GCD study was 350 F g^{-1} at 1 A g^{-1} current density, where the amount of BP added on graphoil was less than 1 mg.

The group of Mahalingam[89] fabricated a symmetric supercapacitor device using 2D-borophene nanosheets anchored S, N-mesoporous carbon nanocomposite (SNC-Bp//SNC-Bp). CV and GCD analyses using 3 M KOH electrolyte in a three-electrode set-up showed an impressive capacitance value of 805.3 F g^{-1} at 10 mV s^{-1} scan rate and 607 F g^{-1} at 1 A g^{-1} current density. The SNC-Bp//SNC-Bp device displayed excellent energy and power density values of 29.2 W h kg^{-1} and 3500 W kg^{-1}, respectively, while retaining 90.67% of the original capacitance and a coulombic efficiency of 91.27%.

Kumar and Vinu's group[54] successfully demonstrated the experimental doping of iron (*ca.* 13%) and sulfur (*ca.* 11%) in

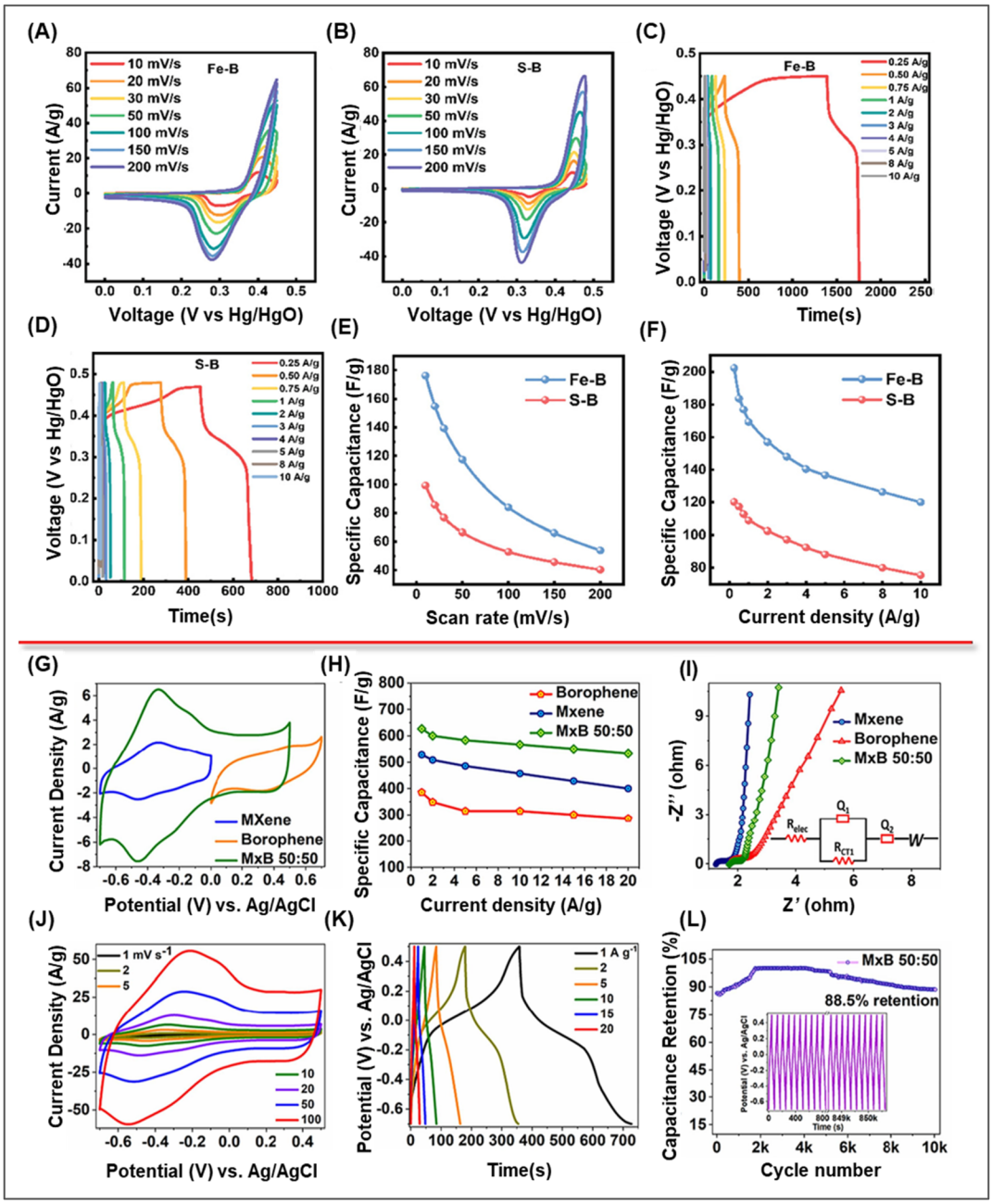

Fig. 9 (A–F) Electrochemical performance of Fe–B and S–B in 6 M KOH electrolyte solution. CV curves of (A) Fe–B and (B) S–B at different scan rates, GCD curves of (C) Fe–B and (D) S–B at different current densities and variation of specific capacitance with (E) scan rate and (F) current density. Reproduced with permission. Copyright 2024, Wiley-VCH GmbH.[54] (G–L) Comparative electrochemical performance of borophene, MXene and MxB (50 : 50) in 2.0 M H_2SO_4. (G) CV curves at a scan rate of 10 mV s^{-1}, (H) specific capacitance at different current densities and (I) Nyquist plots of the samples. (J) CV curves at various scan rates, (K) GCD curves at different current densities and (L) cyclic stability at 10 A g^{-1} for 10 000 cycles of MxB (50 : 50). Reproduced with permission. Copyright 2023, Elsevier B.V.[34]

mono/few-layered β_{12} borophene with exceptional supercapacitive behaviour by controlled microwave exposure technique (Fig. 9A–F). They identified the potential window range for both CV and GCD measurements in a three-electrode system using 6 M KOH electrolyte. They were found to be 0–0.45 V for Fe–B (iron-doped BP) and 0–0.48 V for S–B (sulfur-doped BP). From CV, the values of specific capacitance were calculated to be *ca.* 176 and 99 F g^{-1} at a scan rate of 10 mV s^{-1} and from GCD, the values obtained were 202 and 120 F g^{-1} at a current density of 0.25 A g^{-1} for Fe–B and S–B, respectively. Fe–B and S–B retained 61.1% and 100.5% of their initial capacitance values, respectively, after 5000 CV cycles at 100 mV s^{-1}.

Somesh *et al.*[34] fabricated ultrafast, high-performance flexible supercapacitor electrodes from the heterostructure of 2D MXene/BP (MxB) *via* the electrophoretic deposition method (Fig. 9G–L). To avoid the self-restacking of negatively charged MXene, the positively charged BP was intercalated within the MXene layers. This led to an increase in the interlayer spacing, which exposed more electroactive sites and accelerated the electrolyte ion diffusion as well. In a three-electrode system using 2 M H_2SO_4 electrolyte, the MxB (50 : 50) electrode exhibited a high gravimetric capacitance of 626.7 F g^{-1} at a current density of 1 A g^{-1} with 85.14% retention of capacitance at a high current density of 20 A g^{-1}. This value was greater than that for either MXene (528.5 F g^{-1}, 74.68% capacitance retention) or BP (385.7 F g^{-1}, 71.15% capacitance retention) taken alone. Further, the MxB (50 : 50) electrode displayed remarkable cycling stability with 88.5% capacitance retention after 10 000 cycles. A symmetric solid-state supercapacitor constructed using PVA/H_2SO_4-based gel electrolyte offered an excellent energy density value of 75.6 W h kg^{-1}.

To summarize, the symmetric supercapacitor of a few-layered boron sheet-derived electrode[49] operated in the high potential window of 3.0 V showed an impressive energy density with excellent cyclability. However, as the current density increased, the specific capacitance of this cell decreased, thereby putting a limit to the practical utilization of the material. This suboptimal efficiency poses a serious limitation on its application in high-performance supercapacitors, which demand fast charge/discharge cycles. After the cyclic stability study, the internal resistance increased (from 19.8 Ohm to 22.4 Ohm) to a large extent, which suggested slow ion transfer between the electrode and the electrolyte, thus further restricting its performance. This problem may be overcome by the optimization of the layered structure, porosity of the active material and also the electrolyte, which helps in faster ion diffusion and reduces the internal resistance. These drawbacks excluded, the work provides the advantages of obtaining few-layer B sheets, which can be converted into thin films and composites in bulk with a broad range of applications in flexible electronics, optoelectronics and energy storage devices. On the other hand, the oxygen-defective boron nanosheets[61] gave good pseudocapacitive properties at various pH ranges with a better performance in an acidic medium. This can be attributed to the increase in the interlayer spacing during the oxidative exfoliation, which predisposes better more electroactive sites. Additionally, the oxygen centres functioned as active sites for the adsorption/desorption of ions as well as redox transitions. The corresponding symmetric cell was operated at a high potential window of 3.0 V in ionic electrolyte, but the energy density and recyclability needed improvement.

Again, the active electrodes derived from inorganic/organic nanocomposites of crystalline α BP with PANI[36] and β_{12} BP with PEDOT:PSS[35] showed high capacitance values of 960 and 853 F g^{-1}, respectively, in a three-electrode system and an acidic electrolytic medium. The crystal perfection of the α-phase, due to its low concentration of structural disorders, interstitials and vacancies, enabled high carrier mobility, whereas the high surface area and better structural stability of the β_{12} phase enhanced its charge storage ability. Both the materials showed a capacitance retention of 95% after 1000 cycles. However, to explore the long-term stability, additional tests over extended cycles would be needed to fully comprehend the durability and performance deterioration of the electrodes in practical applications. A facile fabrication process of the supercapacitor was developed by simply depositing BP nanosheets on graphite substrate by the spin-coating method[42] to achieve a specific capacitance of 350 F g^{-1}. In the practical performance using a two-electrode system, the capacitance was observed to be 30% lower than that in the three-electrode system, and during the tests, the morphology of the atomic-thin BP layer was affected. Thus, the strategy of application of a protective layer of another 2D material was suggested, which might stabilize the structure of BP against oxidation and keep the morphology intact.

BP has a serious issue of π–π interaction, leading to the restacking of the sheets and poor ambient stability. To overcome these problems, a unique electrode material was developed based on a nanocomposite that combined S and N-doped mesoporous carbon with BP[89] to provide commendable energy and power densities. The combination of these nanocomposites with other energy storage devices, *e.g.*, batteries, puts forward challenges in terms of compatibility of the materials and optimization of the interfaces. In another approach, flexible supercapacitor electrodes were developed *via* the electrophoretic deposition method with another 2D material, MXene.[34] The negative charge on the surface of MXene and the positive charge of BP electrostatically self-assembled to prevent the restacking problem. This led to a larger interlayer gap between the sheets and exposed more electroactive sites for ion diffusion to provide exceptional energy density (75 W h kg^{-1}) and cycle stability. This work offered a rudimentary insight into the effect of interlayer spacing on the electrochemical properties of 2D hybrid materials and illustrated the design of integrated supercapacitors having high volumetric and rate capabilities. However, the complexity of assembling such 2D materials as well as the high cost involved in the production of high-quality MXene and BP can limit their economic viability, large-scale production and widespread application for commercial supercapacitors at the industrial scale. Also, the environmental stability of the MXene/BP heterostructures in the long-term under various conditions of humidity and temperature has not

been fully understood yet. Thus, research is needed to further develop hybrid systems that effectively integrate the merits of various energy storage technologies.

Separately doping a metal (Fe) and a nonmetal (S) in BP by an innovative one-pot microwave-assisted method[54] not only enhances the electronic properties of the resulting materials but also improves their storage capability significantly. It was necessary to optimize the doping concentration and uniformity of the dopant throughout the entire surface of BP; merely a high doping level did not afford a high specific capacitance value. The potential window of these supercapacitors was very narrow, and the Fe-doped BP suffered from poor recyclability. However, to understand how these dopants influence the energy storage properties of BP, it is essential to fabricate various metals and heteroatoms-doped BP materials and carry out their electrochemical studies.

Comprehensive studies, such as the fabrication of cells that work in high potential window range, determination of energy density and power density and testing the long-term cycling ability are required to evaluate the potential of the supercapacitors in practical applications. Such studies shall also help to precisely identify the benefits and limitations of BP-derived supercapacitor materials by comparison with other similar materials/composites. Future research should prioritize the development of high-performance, lightweight, flexible and portable supercapacitors using BP or BP-based materials based on their exceptional properties such as high electrical conductivity, flexibility and surface area. However, challenges will remain in the scaling up of the production and integrating the materials into devices. It should be kept in mind that BP is highly reactive and prone to aerial oxidation, which can diminish its superiority in the electrochemical performance of supercapacitors. Some effective approaches, such as synthesizing bilayer/tri-layer BP or using protective coatings with another stable 2D material or fabrication of heterostructures with other stable materials, may help to mitigate the issues related to the environmental stability of BP sheets. After the hydrogenation of BP, borophane exhibits remarkable stability in strongly acidic and alkaline medium, which ensures that it can be a potential candidate for various advanced nanoelectronic devices. Ongoing researches aim to optimize these aspects in order to make BP a promising material in sustainable energy storage. Parallelly, attention must be given to minimize the environmental impact and decrease the cost of production and fabrication of devices.

Conclusions and future prospects

Theoretical and experimental studies on borophene have drawn significant attention due to its unique properties such as high anisotropic mechanical characteristics and flexibility, thermal and electronic conductivity, and magnetic properties. Borophene has useful properties such as polymorphism and anisotropy that have contributed to the development of advanced energy materials for research on flexible energy storage systems as supercapacitors. However, several challenges are faced during their implementation in practical applications, such as maintaining high quality and scalability in the synthesis techniques, stability of the structure, tuning of the band gap by optimal strain/defect engineering, chemical functionalization for specific applications and biocompatibility. The bond formation energy of boron is relatively high with a complicated bonding nature arising from the electron deficiency per atom in boron, thereby making it difficult to achieve the monolayer form. The formation of a monolayer of BP needs high surface energy in the bottom-up approach of crystal growth along with higher sonic energy for the exfoliation of boron crystals. Apart from that, the existence of BP in different phases always requires filtration and separation of the phases, which is a matter of concern. BP has been theoretically projected as a befitting material for energy storage and a frontline candidate in catalytic applications. However, the difficulties associated with the synthesis of BP and the practical problems related to achieving it in the monolayer form limit its spectrum of applications.

In the bottom-up strategy, PVD and CVD techniques have the advantage of producing highly pure and stable homogeneous monolayer sheets of BP with good crystallinity and uniform thicknesses. But these processes are very slow, expensive, highly complicated and require highly controlled conditions such as ultra-high vacuum (UHV) and high temperature, making them less accessible for large-scale production. The choice of an appropriate substrate material is delicate as well as crucial for the epitaxial growth or proper deposition in the synthesis of the individual phases of BP. Again, BP layers establish weak interaction with the substrate, as a result of which the separation process becomes difficult and leads to the damage of the BP sheets. In some cases, strain can be induced in the BP structure by the substrate, resulting in further complications of the separation process. Such strain can give rise to defects and even structural changes in BP, making it more difficult to accomplish a clean separation. In this regard, the van der Waals epitaxial method where the BP growth takes place over a non-metallic substrate, such as mica, may open up new possibilities for introducing BP in various electronic applications, but it may not be easily scalable for large-scale production. Segregation-enhanced epitaxial method affords large-area BP domains with high quality and low defect density. This is important for practical applications as larger domains can enhance the performance of BP-based devices. This segregation process again involves its own limitations; when a certain quantity of BP is produced by the segregation of boron on the surface of the substrate, further growth may be inhibited. In addition, it requires very high temperatures (up to 1373 K) and there are issues related to the solubility constraint of boron. All these factors must be taken into account while considering the feasibility and scalability of a given synthetic approach. Thus, more research is needed for the large-scale production of BP with a high degree of reproducibility, which is essential for practical applications.

On the other hand, different exfoliation techniques such as liquid phase exfoliation, mechanical exfoliation, and electro-

chemical exfoliation are easier, scalable and more cost-effective to achieve free-standing BP sheets. However, the quality and purity of the BP obtained is not as high as that in the CVD and MBE techniques, and it is very difficult to maintain the size and thickness of the BP. Innovations can be brought in the exfoliation techniques, such as exploring high-energy solvents (DMF, DMSO, NMP, *etc.*), using solvent mixtures (DMF/IPA, NMP/ethanol, acetone/IPA, *etc.*), studying the effect of heating while sonication, and trying vacuum exfoliation or cryo-exfoliation. As research on borophene spreads across different technological applications, a closer understanding of the surface, as well as interface chemistry, is vital, particularly for their potential applications in devices, which are quite restricted at present. Micromechanical exfoliation technique leads to high-quality BP, but the uniformity of the number of layers is always a prime concern, which greatly affects the electronic and mechanical properties of BP sheets. The modified Hummers' method appears as a step forward in this direction, thus pushing the boundary further. The yield of BP in the modified Hummers' method has been found to be the best so far and the method is very much suitable for the large-scale production of BP, which is desirable in energy storage or catalytic applications. However, it experiences problems related to defects and surface functionalities with the contamination of BP sheets by oxidized BP. Thus, there is still a lot of opportunity to design a more effective synthetic route of BP, which will ensure scalability without compromising on its quality as well as precise control of the structures, purity, crystallinity, size and homogeneity.

Borophene is oxidized on exposure to air or moisture, which leads to the weakening of its valuable properties. Again, by hydrogen functionalization, its stability increases and the hydrogenated BP has greater thermal conductivity than pristine BP. However, the bilayer BP displays a metallic character and compared to the monolayer forms, it is less susceptible towards oxidation. The ability to tailor the bandgap of BP *via* controlled strain/defect engineering or by chemical treatment on its surface is one of the most fascinating features that modulates the metallic to semiconducting behaviour of BP. Its excellent electrical conductivity, strong mechanical flexibility, low diffusion barrier, lightweight, tuneable band gap and high theoretical conductance make BP a potential candidate in supercapacitors for flexible energy storage systems.

Recent research endeavours have concentrated on the unique properties exhibited by 2D heterostructures involving direct interfaces between components that are chemically distinct. These interfaces play a crucial role in boosting the charge storage capacities through synergistic interactions. Nevertheless, the fabrications of such stable heterostructures offer their own set of challenges. BP has the compatibility to form heterostructures with other 2D materials, such as MXene or conductive polymers such as PANI and PEDOT:PSS/β_{12}, due to its polymorphism and diverse bonding geometries. The formation of such heterostructures prevents the self-restacking of the BP sheets and facilitates the composites to serve as effective electrode materials for supercapacitors. To date, the field of BP-derived supercapacitors has not been explored much and the charge storage mechanism of BP-based electrodes, including the various phenomena taking place at the interface of the electrode/electrolyte, are active areas of research. Therefore, further study in this field is required to explore the energy storage capability of the heterostructures with other 2D materials such as graphene, phosphorene, transition metal dichalcogenides and black phosphorus as well as different dopants and various conductive polymers.

Future research directions can focus on the development of economic, time-effective and scalable production of highly pure BP and the fabrication of nanocomposite electrode materials for supercapacitors with good mechanical stability, flexibility, lightweight, high-energy density, power density, rapid charge/discharge kinetics and recyclability. Lightweight, fire-resistant and high-power supercapacitors are suitable for different types of light electronic gadgets and electrical vehicles. In addition to supercapacitors, BP or BP-based materials can have emerging applications in the field of lithium-ion batteries, electrocatalysts (water splitting), sensors (gas, molecule, fire, strain, *etc.*), photodetectors, biomedicines (cancer therapy, diabetic sensing, *etc.*), information technology, wireless communication, hydrogen storage, electrical transport, field emission, and so on. There is a vast expanse remaining unexplored, which provides ample opportunities to carry out useful research in this area and meet the challenges faced in utilization of renewable energy through the development of efficient energy storage systems.

Data availability

The data will be available from the authors on request.

Conflicts of interest

There are no conflicts to declare.

Acknowledgements

PP wishes to thank UGC, New Delhi for providing fellowship. MN gratefully acknowledges financial support from CSIR, New Delhi (sanction letter no. 01(3088)/21/EMR-II).

References

1 Y. Chao, Y. Han, Z. Chen, D. Chu, Q. Xu, G. Wallace and C. Wang, *Adv. Sci.*, 2024, **11**, 2305558.
2 H. Bin Wu and X. W. Lou, *Sci. Adv.*, 2017, **3**, eaap9252.
3 B. Dunn, H. Kamath and J.-M. Tarascon, *Science*, 2011, **334**, 928–935.
4 P. Simon and Y. Gogotsi, *Nat. Mater.*, 2008, **7**, 845–854.
5 J. Yan, Q. Wang, T. Wei and Z. Fan, *Adv. Energy Mater.*, 2014, **4**, 1300816.

6 X. Huang, X. Qi, F. Boey and H. Zhang, *Chem. Soc. Rev.*, 2012, **41**, 666–686.
7 X. Huang, Z. Yin, S. Wu, X. Qi, Q. He, Q. Zhang, Q. Yan, F. Boey and H. Zhang, *Small*, 2011, **7**, 1876–1902.
8 C. Yan, Y.-L. Liu, Q. Zeng, G.-G. Wang and J.-C. Han, *Adv. Funct. Mater.*, 2023, **33**, 2210837.
9 R. Kumar, S. Sahoo, E. Joanni, R. Pandey and J.-J. Shim, *Chem. Commun.*, 2023, **59**, 6109–6127.
10 S. Suragtkhuu, S. Sunderiya, P. Myagmarsereejid, S. Purevdorj, A. S. R. Bati, B. Bold, Y. L. Zhong, S. Davaasambuu and M. Batmunkh, *Adv. Energy Mater.*, 2023, **13**, 2204074.
11 W. Waheed, S. Anwer, M. U. Khan, M. Sajjad and A. Alazzam, *Chem. Eng. J.*, 2024, **480**, 147981.
12 K. S. Novoselov, A. K. Geim, S. V. Morozov, D. Jiang, Y. Zhang, S. V. Dubonos, I. V. Grigorieva and A. A. Firsov, *Science*, 2004, **306**, 666–669.
13 A. K. Geim, *Science*, 2009, **324**, 1530–1534.
14 A. Carvalho, M. Wang, X. Zhu, A. S. Rodin, H. Su and A. H. C. Neto, *Nat. Rev. Mater.*, 2016, **1**, 16061.
15 M. Pumera, Z. Sofer and A. Ambrosi, *J. Mater. Chem. A*, 2014, **2**, 8981–8987.
16 Y.-Z. Zhang, J. K. El-Demellawi, Q. Jiang, G. Ge, H. Liang, K. Lee, X. Dong and H. N. Alshareef, *Chem. Soc. Rev.*, 2020, **49**, 7229–7251.
17 Q. Weng, X. Wang, X. Wang, Y. Bando and D. Golberg, *Chem. Soc. Rev.*, 2016, **45**, 3989–4012.
18 L. Li, Y. Yu, G. J. Ye, Q. Ge, X. Ou, H. Wu, D. Feng, X. H. Chen and Y. Zhang, *Nat. Nanotechnol.*, 2014, **9**, 372–377.
19 A. J. Mannix, X.-F. Zhou, B. Kiraly, J. D. Wood, D. Alducin, B. D. Myers, X. Liu, B. L. Fisher, U. Santiago, J. R. Guest, M. J. Yacaman, A. Ponce, A. R. Oganov, M. C. Hersam and N. P. Guisinger, *Science*, 2015, **350**, 1513–1516.
20 A. J. Mannix, Z. Zhang, N. P. Guisinger, B. I. Yakobson and M. C. Hersam, *Nat. Nanotechnol.*, 2018, **13**, 444–450.
21 Z. Zhang, E. S. Penev and B. I. Yakobson, *Chem. Soc. Rev.*, 2017, **46**, 6746–6763.
22 Z. Wu, G. Tai, A. R. Liu, S. W. Shao, C. Hou and X. Liang, *J. Mater. Chem. A*, 2022, **10**, 8218–8226.
23 C. Hou, G. Tai, Y. Liu, Z. Wu, X. Liang and X. Liu, *Nano Res. Energy*, 2023, **2**, e9120051.
24 C. Hou, G. Tai, J. Hao, L. Sheng, B. Liu and Z. Wu, *Angew. Chem., Int. Ed.*, 2020, **59**, 10819–10825.
25 Y. V. Kaneti, D. P. Benu, X. Xu, B. Yuliarto, Y. Yamauchi and D. Golberg, *Chem. Rev.*, 2022, **122**, 1000–1051.
26 E. S. Penev, A. Kutana and B. I. Yakobson, *Nano Lett.*, 2016, **16**, 2522–2526.
27 H. Chand, A. Kumar and V. Krishnan, *Adv. Mater. Interfaces*, 2021, **8**, 2100045.
28 Y. Liu, E. S. Penev and B. I. Yakobson, *Angew. Chem., Int. Ed.*, 2013, **52**, 3156–3159.
29 G. J. Adekoya, O. C. Adekoya, M. Muloiwa, E. R. Sadiku, W. K. Kupolati and Y. Hamam, *Small*, 2024, 2403656.
30 C. Hou, G. Tai, Z. Wu and J. Hao, *ChemPlusChem*, 2020, **85**, 2186–2196.
31 B. Mortazavi, M. Makaremi, M. Shahrokhi, M. Raeisi, C. V. Singh, T. Rabczuk and L. F. C. Pereira, *Nanoscale*, 2018, **10**, 3759–3768.
32 C. Zhan, P. Zhang, S. Dai and D. Jiang, *ACS Energy Lett.*, 2016, **1**, 1241–1246.
33 S. Faramarzi and T. Movlarooy, *ACS Appl. Mater. Interfaces*, 2024, **16**, 25966–25976.
34 T. E. Somesh, D. T. Tran, S. Jena, Y. Bai, S. Prabhakaran, D. H. Kim, N. H. Kim and J. H. Lee, *Chem. Eng. J.*, 2024, **481**, 148266.
35 T. A. Türkmen, N. Taşaltın, C. Taşaltın, G. Baytemir and S. Karakuş, *Inorg. Chem. Commun.*, 2022, **139**, 109329.
36 S. Göktuna and N. Taşaltın, *Phys. E*, 2021, **134**, 114833.
37 M. Ou, X. Wang, L. Yu, C. Liu, W. Tao, X. Ji and L. Mei, *Adv. Sci.*, 2021, **8**, 2001801.
38 G. H. Gupta, S. Kadakia, D. Agiwal, T. Keshari and S. Kumar, *Mater. Adv.*, 2024, **5**, 1803–1816.
39 S. Yadav, M. A. Sadique, A. Kaushik, P. Ranjan, R. Khan and A. K. Srivastava, *J. Mater. Chem. B*, 2022, **10**, 1146–1175.
40 J. Joseph, V. S. Sivasankarapillai, S. Nikazar, M. S. Shanawaz, A. Rahdar, H. Lin and G. Z. Kyzas, *ChemSusChem*, 2020, **13**, 3754–3765.
41 G. Tai, M. Xu, C. Hou, R. Liu, X. Liang and Z. Wu, *ACS Appl. Mater. Interfaces*, 2021, **13**, 60987–60994.
42 Y. Abdi, A. Mazaheri, S. Hajibaba, S. Darbari, S. J. Rezvani, A. D. Cicco, F. Paparoni, R. Rahighi, S. Gholipour, A. Rashidi, M. M. Byranvand and M. Saliba, *ACS Mater. Lett.*, 2022, **4**, 1929–1936.
43 Z. Guo, H. Lin, H. Zhang, Y. Tian, Y. Chen, J. Chen, S. Deng and F. Liu, *Cryst. Growth Des.*, 2023, **23**, 4506–4513.
44 S. J. Rezvani, Y. Abdi, R. Parmar, F. Paparoni, S. Antonini, R. Gunnella, A. D. Cicco, M. Amati, L. Gregoratti, A. Mazaheri and S. Hajibaba, *ACS Appl. Nano Mater.*, 2024, **7**, 13712–13719.
45 B. Feng, J. Zhang, Q. Zhong, W. Li, S. Li, H. Li, P. Cheng, S. Meng, L. Chen and K. Wu, *Nat. Chem.*, 2016, **8**, 563–568.
46 C. Chen, H. Lv, P. Zhang, Z. Zhuo, Y. Wang, C. Ma, W. Li, X. Wang, B. Feng, P. Cheng, X. Wu, K. Wu and L. Chen, *Nat. Chem.*, 2022, **14**, 25–31.
47 K. M. Omambac, M. Petrović, P. Bampoulis, C. Brand, M. A. Kriegel, P. Dreher, D. Janoschka, U. Hagemann, N. Hartmann, P. Valerius, T. Michely, F. J. M. Heringdorf and M. H. Hoegen, *ACS Nano*, 2021, **15**, 7421–7429.
48 Z. Wu, G. Tai, R. Liu, C. Hou, W. Shao, X. Liang and Z. Wu, *ACS Appl. Mater. Interfaces*, 2021, **13**, 31808–31815.
49 H. Li, L. Jing, W. Liu, J. Lin, R. Y. Tay, S. H. Tsang and E. H. T. Teo, *ACS Nano*, 2018, **12**, 1262–1272.
50 X. Ji, N. Kong, J. Wang, W. Li, Y. Xiao, S. T. Gan, Y. Zhang, Y. Li, X. Song, Q. Xiong, S. Shi, Z. Li, W. Tao, H. Zhang, L. Mei and J. Shi, *Adv. Mater.*, 2018, **30**, 1803031.
51 D. Ma, R. Wang, J. Zhao, Q. Chen, L. Wu, D. Li, L. Su, X. Jiang, Z. Luo, Y. Ge, J. Li, Y. Zhang and H. Zhang, *Nanoscale*, 2020, **12**, 5313–5323.

52 L. Guo, H. Wang, Z. Wu, X. Yang, R. Ma, Y. Hu, G. Li, D. Shi, W. Xie, W. Zhang, F. Lan, L. Zhou and K. Zhang, *Chem. Eng. J.*, 2023, **473**, 145017.
53 S. Radhakrishnan, N. T. Padmanabhan, A. J. Mathews, Y. Tang, T. Santhanakrishnan and H. John, *ACS Appl. Nano Mater.*, 2024, **7**, 12564–12578.
54 Z. Li, X. Guan, G. Pandey, S. Chahal, A. Bandyopadhyay, K. Awasthi, P. Kumar and A. Vinu, *Small*, 2024, 2307610.
55 S. Chahal, P. Ranjan, M. Motlag, S. S. R. K. C. Yamijala, D. J. Late, E. H. S. Sadki, G. J. Cheng and P. Kumar, *Adv. Mater.*, 2021, **33**, 2102039.
56 K. Zielinkiewicz, D. Baranowska and E. Mijowska, *RSC Adv.*, 2023, **13**, 16907–16914.
57 K. Zielinkiewicz and E. Mijowska, *Sustainable Mater. Technol.*, 2024, **39**, e00860.
58 K. Sielicki, K. Maślana, X. Chen and E. Mijowska, *Sci. Rep.*, 2022, **12**, 15683.
59 M. A. Chowdhury, M. M. K. Uddin, M. B. A. Shuvho, M. Rana and N. Hossain, *Appl. Surf. Sci. Adv.*, 2022, **11**, 100308.
60 P. Ranjan, T. K. Sahu, R. Bhushan, S. S. R. K. C. Yamijala, D. J. Late, P. Kumar and A. Vinu, *Adv. Mater.*, 2019, **31**, 1900353.
61 A. Joshi, A. K. Tomar, G. Singh and R. K. Sharma, *Chem. Eng. J.*, 2021, **407**, 127122.
62 Z. Zhang, Y. Yang, E. S. Penev and B. I. Yakobson, *Adv. Funct. Mater.*, 2017, **27**, 1605059.
63 S. Sadeghzadeh, *Comput. Mater. Sci.*, 2018, **143**, 1–14.
64 Z. Wang, T.-Y. Lü, H.-Q. Wang, Y. P. Feng and J.-C. Zheng, *Phys. Chem. Chem. Phys.*, 2016, **18**, 31424–31430.
65 H. Sun, Q. Li and X. G. Wan, *Phys. Chem. Chem. Phys.*, 2016, **18**, 14927–14932.
66 H. Zhou, Y. Cai, G. Zhang and Y.-W. Zhang, *npj 2D Mater. Appl.*, 2017, **1**, 14.
67 B. Liu and K. Zhou, *Prog. Mater. Sci.*, 2019, **100**, 99–169.
68 P. Roy, S. Ghoshal, A. Pramanik and P. Sarkar, *Phys. Chem. Chem. Phys.*, 2023, **25**, 25018–25028.
69 H. Xiao, W. Cao, T. Ouyang, S. Guo, C. He and J. Zhong, *Sci. Rep.*, 2017, **7**, 45986.
70 B. Mortazavi, M.-Q. Le, T. Rabczuk and L. F. C. Pereira, *Phys. E*, 2017, **93**, 202–207.
71 J. F. N. Dethan, *Phys. Chem. Chem. Phys.*, 2021, **23**, 17009–17017.
72 Z. Wang, T.-Y. Lü, H.-Q. Wang, Y. P. Feng and J.-C. Zheng, *Sci. Rep.*, 2017, **7**, 609.
73 X. Tang, J. Gu, J. Shang, Z. Chen and L. Kou, *InfoMat*, 2021, **3**, 327–336.
74 Y. He, N. Cheng, C. Chen, S. Xiong and J. Zhao, *Sci. China: Technol. Sci.*, 2019, **62**, 799–810.
75 A. A. Kistanov, Y. Cai, K. Zhou, N. Srikanth, S. V. Dmitriev and Y.-W. Zhang, *Nanoscale*, 2018, **10**, 1403–1410.
76 B. N. Šoškić, J. Bekaert, C. Sevik and M. V. Milošević, *Nano Lett.*, 2024, **24**, 12650–12657.
77 Q. Li, L. Wang, H. Li, M. K. Y. Chan and M. C. Hersam, *ACS Nano*, 2024, **18**, 483–491.
78 C. Zhang, Z. Zhang, W. Yan and X. Qin, *Adv. Condens. Matter Phys.*, 2021, **1**, 3718040.
79 J. Jiang, X. Wang and Y. Song, *Comput. Mater. Sci.*, 2018, **153**, 10–15.
80 J.-H. Liao, Y.-C. Zhao, Y.-J. Zhao, H. Xu and X.-B. Yang, *Phys. Chem. Chem. Phys.*, 2017, **19**, 29237–29243.
81 A. Pal, P. Pal and M. Nandi, *Energy Fuels*, 2023, **37**, 9568–9581.
82 P. Pal, S. Bhowmik and M. Nandi, *Chem. – Eur. J.*, 2024, **30**, e202400638.
83 M. Pal, S. Bhowmik and M. Nandi, *New J. Chem.*, 2024, **48**, 16931–16947.
84 A. Noori, M. F. El-Kady, M. S. Rahmanifar, R. B. Kaner and M. F. Mousavi, *Chem. Soc. Rev.*, 2019, **48**, 1272–1341.
85 Y. Wang, Y. Song and Y. Xia, *Chem. Soc. Rev.*, 2016, **45**, 5925–5950.
86 P. Pal, A. Pal, M. Pal and M. Nandi, *ACS Appl. Nano Mater.*, 2024, **7**, 22975–22988.
87 C. Zhong, Y. Deng, W. Hu, J. Qiao, L. Zhang and J. Zhang, *Chem. Soc. Rev.*, 2015, **44**, 7484–7539.
88 M. Pal, A. Pal, P. Pal and M. Nandi, *ACS Appl. Eng. Mater.*, 2023, **1**, 2965–2983.
89 D. K. Chinnalagu, B. Murugesan, M. Arumugam, K. Chinniah, S. Ganesan, Y. Cai and S. Mahalingam, *J. Energy Storage*, 2023, **74**, 109328.

